ADVANCED MATERIALS
www.advmat.de

Localized Nanoparticle-Mediated Delivery of miR-29b Normalizes the Dysregulation of Bone Homeostasis Caused by Osteosarcoma whilst Simultaneously Inhibiting Tumor Growth

Fiona E. Freeman, Pere Dosta, Lianne C. Shanley, Natalia Ramirez Tamez, Cristobal J. Riojas Javelly, Olwyn R. Mahon, Daniel J. Kelly, and Natalie Artzi**

Patients diagnosed with osteosarcoma undergo extensive surgical intervention and chemotherapy resulting in dismal prognosis and compromised quality of life owing to poor bone regeneration, which is further compromised with chemotherapy delivery. This study aims to investigate if localized delivery of miR-29b—which is shown to promote bone formation by inducing osteoblast differentiation and also to suppress prostate and cervical tumor growth—can suppress osteosarcoma tumors whilst simultaneously normalizing the dysregulation of bone homeostasis caused by osteosarcoma. Thus, the therapeutic potential of microRNA (miR)-29b is studied to promote bone remodeling in an orthotopic model of osteosarcoma (rather than in bone defect models using healthy mice), and in the context of chemotherapy, that is clinically relevant. A formulation of miR-29b:nanoparticles are developed that are delivered via a hyaluronic-based hydrogel to enable local and sustained release of the therapy and to study the potential of attenuating tumor growth whilst normalizing bone homeostasis. It is found that when miR-29b is delivered along with systemic chemotherapy, compared to chemotherapy alone, the therapy provided a significant decrease in tumor burden, an increase in mouse survival, and a significant decrease in osteolysis thereby normalizing the dysregulation of bone lysis activity caused by the tumor.

1. Introduction

Osteosarcoma is a highly aggressive bone cancer, largely affecting children and adolescents with a worldwide incidence rate of 26 000 new cases per year.[1] Due to the young age of initial diagnosis, the management of this disease is a challenging and costly exercise, estimated to be €14.7 billion in Europe in the last 18 years.[2] Despite significant advances in treatment seen in other malignancies, no major improvements in outcomes have been achieved since the introduction of chemotherapy in the 1970s.[3] Contemporary chemotherapy is usually administered to the patient with three cycles prior to tumor resection and three cycles post tumor resection. However, these chemotherapeutic drugs have a series of short and long-term side effects on the patients and are not curative.[4] This emphasizes the strong clinical unmet need for newer, more effective, treatment options to improve the overall survival of these young patients.[5] Furthermore, as osteosarcoma is such an aggressive disease, the surgical

F. E. Freeman, L. C. Shanley, O. R. Mahon, D. J. Kelly
Trinity Centre for Biomedical Engineering
Trinity Biomedical Sciences Institute
Trinity College Dublin
Dublin D02 PN40, Ireland
E-mail: fiona.freeman@ucd.ie

F. E. Freeman, D. J. Kelly
Department of Mechanical
Manufacturing, and Biomedical Engineering
School of Engineering
Trinity College Dublin
Dublin D02 PN40, Ireland

The ORCID identification number(s) for the author(s) of this article can be found under https://doi.org/10.1002/adma.202207877

DOI: 10.1002/adma.202207877

F. E. Freeman, P. Dosta, N. Artzi
Institute for Medical Engineering and Science
Massachusetts Institute of Technology
Cambridge, MA 02139, USA
E-mail: nartzi@bwh.harvard.edu

F. E. Freeman, P. Dosta, N. Ramirez Tamez, C. J. Riojas Javelly, N. Artzi
Department of Medicine
Division of Engineering in Medicine
Brigham and Women's Hospital
Harvard Medical School
Boston, MA 02115, USA

F. E. Freeman, L. C. Shanley, D. J. Kelly
Advanced Materials and Bioengineering Research Centre (AMBER)
Royal College of Surgeons in Ireland and Trinity College Dublin
Dublin D02 YN77, Ireland

F. E. Freeman
School of Mechanical and Materials Engineering
Engineering and Materials Science Centre
University College Dublin
Dublin D04 V1W8, Ireland

intervention usually involves total reconstruction of the limbs or in most cases amputation. To add to this, both chemotherapeutics and osteosarcoma tumors have been shown to disrupt bone homeostasis,[6] resulting in a dysregulated bone lysis activity significantly hindering the surrounding bone's ability to regenerate following surgical intervention. Therefore, any bone regeneration strategy that would stimulate the bone remodeling process, within the surrounding bone following surgical intervention, would be of great interest to these young patients. Yet, there exists a fine balance between trying to promote bone remodeling and promoting tumor growth, which has significantly slowed down fundamental research and clinical translation of tissue engineering strategies for cancer patients.[7]

The controlled in vivo delivery of microRNAs (miRNAs), noncoding small RNAs that regulate gene expression, offer numerous therapeutic advantages and may potentially be developed to target both tumor suppression and promote bone remodeling. miRNAs have been identified as gene expression master regulators and constitute an attractive target for treating cancer as they have been shown to regulate biological systems such as stemness, immunity and have been shown to play a crucial role in the initiation and progression of numerous cancers.[8] miR-29 consists of three mature members, miR-29a, miR-29b and miR-29c, which are encoded in two genetic clusters.[9] Members of this family, specifically miR-29b, have been shown to be silenced or down-regulated in many different types of cancer.[10] Subsequently, restoration of miR-29b has been found to elicit tumor-suppressive properties in a variety of cancers,[10b,d,e,11] but has not been studied in the context of osteosarcoma. It has also been shown that miR-29b plays a key role in bone remodeling by promoting osteoblast differentiation by downregulating TGF-β3 signaling,[12] providing new insight into the use of miRNAs to induce bone formation. Furthermore, as miR-29b has also been shown to inhibit angiogenesis by targeting VEGF signaling pathways,[13] it has the potential to aid in bone regeneration without enhancing vascularisation and thus tumor growth or metastasis. However, the therapeutic potential of miR-29b in osteosarcoma remains unknown. In vitro studies have shown that miR-29b delivery suppresses proliferation and migration and induces apoptosis of osteosarcoma cells[14] and in some cases can sensitize the cells to chemotherapy.[14b,15] Although informative, these studies used 2D in vitro cultures.

There are also several challenges that limit miRNA delivery as a potential treatment option for osteosarcoma. These challenges include poor penetration of miRNAs into the tumor tissues, fast degradation time of unmodified miRNAs, and activation of the innate immune system leading to unexpected toxicities and undesirable side effects.[16] Injectable hydrogels as the miRNA delivery systems have become a research hotspot as they can efficiently avoid these problems by releasing the miRNA locally at the tumor site. By locally delivering the miRNA to the primary tumor site one can achieve superior transfection due to higher bioavailability, and reduced toxicity caused by nonspecific uptake of the miRNA by normal healthy organs.[16] Other advantages of injectable hydrogels include their tuneable properties, controllable degradation, high water content, and shear thinning capabilities allowing them to be injected through a syringe to deliver miRNAs in a minimally invasive manner.[17] As hyaluronic acid (HA) is biocompatible, non-immunogenic, and Food and Drug Administration (FDA)-approved[18] hydrogel and we have previously developed an HA-based microneedle platform for non-invasive immunoregulation in skin transplants,[19] we chose HA as our base hydrogel for the injectable delivery system. We also developed poly-beta-amino-esters (pBAE) nanoparticles as the intracellular delivery vehicle to deliver the miRNA as they have low toxicity and high biocompatibility due to their backbone of repeating ester groups that are biodegradable through hydrolysis in the cell cytoplasm.[20] Unlike lipid-based nanoparticles, which encapsulate the miRNAs within the liposome or micelle structure, pBAE polymeric chains electrostatically interact with the RNA therapeutics as the nanoparticle is self-assembled, allowing for higher encapsulation and loading efficiencies.[21] Previous studies have demonstrated effective delivery of miR-29b via intertumoral injection or local administration of miR-29b via nanoparticle-mediated transfection.[10b,22] Both studies demonstrated the therapeutic potential of localized miR-29b delivery at suppressing tumor growth in both prostate and cervical cancer.[10b,22] Despite these promising results, no study has investigated the therapeutic potential of localized miR-29b delivery in suppressing tumor growth in osteosarcoma.

With this in mind, the overall goal of this study was to investigate if localized delivery of pBAE nanoparticles containing miR-29b to the primary tumor site, along with systemic delivery of chemotherapy, would suppress tumor growth whilst simultaneously providing the surrounding damaged bone the cues needed to normalize bone homeostasis even in the presence of chemotherapy (**Figure 1**). A pBAE nanoparticle delivery vector was developed and tested to efficiently deliver miR-29b to both osteosarcoma cells and surrounding stromal cells in vitro and in vivo. Using our previously developed in vitro spheroid model for osteosarcoma,[7] we validated the therapeutic capabilities of miR-29b delivery in a controlled predictive model of the disease. Upon developing a pre-clinical metastatic murine model for osteosarcoma, we investigated the antitumor efficacy of localized delivery of miR-29b-complexes using an HA-based injectable system to enable efficient, local and sustained release of miR-29b to the primary tumor site. This allowed us to test the true therapeutic potential of the treatment in a diseased orthotopic model.

F. E. Freeman
Conway Institute of Biomolecular and Biomedical Research
University College Dublin
Dublin D04 V1W8, Ireland
P. Dosta, N. Artzi
Wyss Institute for Biologically Inspired Engineering
Harvard University
Boston, MA 02115, USA
L. C. Shanley
School of Biochemistry and Immunology
Trinity College Dublin
Dublin D02 PN40, Ireland
O. R. Mahon
School of Medicine
University of Limerick
Limerick V94 T9PX, Ireland
D. J. Kelly
Department of Anatomy
Royal College of Surgeons in Ireland
Dublin D02 YN77, Ireland

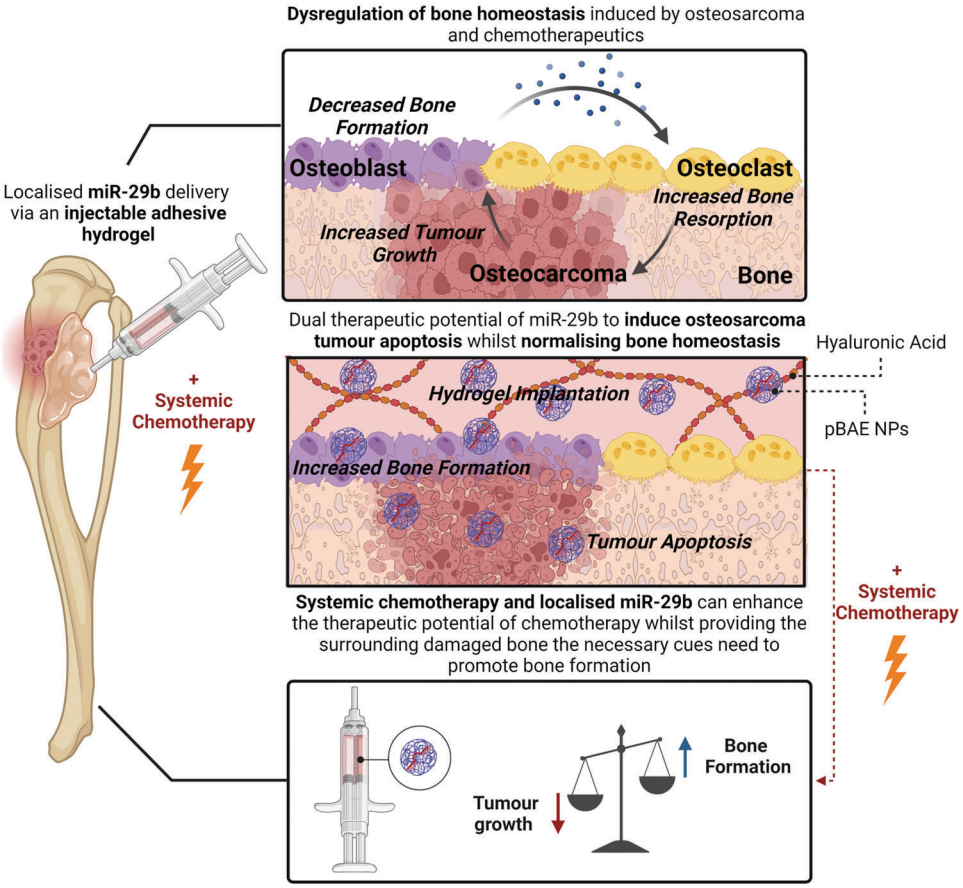

Figure 1. Schematic of the proposed dual-therapeutic role localized delivery of miR-29b:pBAE nanoparticles have in treating osteosarcoma. This will be achieved by inducing apoptosis in the tumor locally by restoring miR-29b expression within the tumor cells whilst simultaneously providing the surrounding damaged bone the cues needed to normalize the dysregulation of bone homeostasis caused by both the chemotherapeutics and the tumor. Created with Biorender.com.

The therapeutic potential was directly compared to and added as a potential add-on to the current clinical gold standard of systemic chemotherapeutic, Doxorubicin, to validate if the therapy can normalize the dysregulation of bone homeostasis caused by both the chemotherapeutics and osteosarcoma. Finally, as bone morphogenic protein-2 (BMP-2) is known to be a strong inducer of bone remodeling,[23] we directly compared our miR-29b treatment to BMP-2 delivery and validated its ability to normalize bone homeostasis and induce bone remodeling. We found that when miR-29b was delivered along with systemic chemotherapy, compared to chemotherapy alone, our therapy provided a significant decrease in tumor burden (45% reduction in tumor volume), an increase in mouse survival (50% survival went from 24 days to 32 days), and a significant decrease in osteolysis (75% reduction in osteolysis) thereby normalizing the dysregulation of bone lysis activity caused by the tumor. When directly compared to BMP-2 delivery, miR-29b significantly reduced osteolysis caused by the tumor and led to enhanced bone tissue distribution, even in the presence of chemotherapy. Together, our study highlights the therapeutic potential of miRNAs, specifically miR-29b, as a novel therapeutic add-on to conventional chemotherapy for targeting not only the primary tumor but also normalizing the dysregulation of bone homeostasis in the surrounding damaged bone.

2. Results

2.1. Synthesis and Characterization of pBAE Nanoparticles

Synthesis of pBAEs was performed via a two-step procedure, as previously reported.[24] First, the addition reaction of primary amines to an excess of diacrylates was used to synthesize an acrylate-terminated polymer (C6 polymer). Then, C6-CR3 polymer was generated by reacting terminal acrylate groups from C6 polymer with thiol-terminated arginine polypeptide (Figure S1A, Supporting Information). C6-CR3 polymer was purified by precipitation and its molecular structure was characterized by ^{1}H-NMR. The chemical structure of the resultant polymer was confirmed by the presence of signals associated with the conjugated arginine peptide (Figure S1B, Supporting Information). We have previously confirmed that the C6-CR3 polymer was able to efficiently complex different types of nucleic acids, from small RNAi[20,25] to DNA plasmids.[26] Here, the miR-29b complexation efficacy using C6-CR3 polymer was evaluated by agarose gel electrophoresis at different C6-CR3:miR-29b ratios (w/w). Complexation of C6-CR3 polymer with miR-29b revealed free miR-29b at ratios below 50:1 C6-CR3:miR-29b (w/w), while at a ratio of 50:1 or higher complete miR-29b complexation was observed

(Figure S1D, Supporting Information). At a 100:1 ratio, the average nanoparticle size was 151 ± 2 nm and the surface charge was 5.6 ± 3.5 mV. The miR-29b nanoparticles were stable for more than 5 days in phosphate buffer solution (PBS). In contrast, at lower polymer:miR-29b ratios the nanoparticle stability was reduced (Figure S1E, Supporting Information). Therefore, the 100:1 C6-CR3:miR-29b ratio was selected for the in vitro and in vivo experiments.

2.2. PBAE-Nanoparticle-Mediated Transfection of Human MSCs Induces a Pro-Osteogenic and Anti-Angiogenic Response Whilst Transfection of Osteosarcoma Cells (Murine and Human) Induces a Pro-Apoptotic Response Alone

To analyze what effect miR-29b delivery would have on human mesenchymal stem cells (MSCs), fluorescently labeled C6-CR3 polymer was complexed with either miR-29b or scrambled miRNA (20 nM, 8.3 μg mL^{-1}) (**Figure 2**A). Following a 4 h transfection with pBAE nanoparticles (Scramble; miR-29b), MSCs were cultured in osteogenic medium for 7 days and then analyzed for DNA content and Annexin V/PI co-staining (biocompatability), alkaline phosphatase (ALP) Activity (pro-osteogenic effect), and vascular endothelial growth factor (VEGF) release (anti-angiogenic effect). Confocal imaging validated cellular uptake of the pBAE nanoparticles 4 h after transfection (Figure 2B). There was no significant difference in DNA content and flow cytometry of apoptotic cell death corroberated this finding with no significant difference in the percentage of cells undergoing apoptosis following miR-29b transfection. On the other hand,there was a significant increase in ALP expression and a significant decrease in VEGF release following miR-29b transfection when compared to the non-transfected and scrambled controls (Figure 2C; Figure S2A,D, Supporting Information).

To understand what effect miR-29b delivery would have on osteosarcoma cells, human osteosarcoma cells (SaOS2) were transfected with pBAE nanoparticles loaded with either scrambled miRNA or miR-29b. Following a 4 h transfection period, the cells were cultured in osteogenic medium for 3 days and then analyzed for DNA content and Annexin V/PI co-staining (pro-apoptotic effect), and ALP Activity. Confocal imaging validated cellular uptake of the pBAE nanoparticles 4 h after transfection (Figure 2D). There was a significant decrease in DNA content following miR-29b transfection when compared to the non-transfected and scrambled controls (Figure 2E). There was also a trend toward an increase ($p = 0.08$) in the percentage of cells undergoing early apoptosis (Q2) and a decrease in viable cells (Q4) in SaOS2 cells 3 days post miR-29b transfection when compared to the scrambled control (Figure S2B,D, Supporting Information). There was no significant difference in ALP activity between all three groups (Figure 2E). Osteosarcoma cells released negligible VEGF over the 3 days (data not shown).

Finally, a K7M2 cell line was chosen as it is considered highly aggressive with a reported pulmonary metastatic rate of over 90% in mice.[27] To ensure that miR-29b has a similar therapeutic response in murine cells as it does in human osteosarcoma cells, K7M2 cells were transfected with pBAE nanoparticles (Scramble; miR-29b). Following a 4 h transfection period, K7M2 cells were further cultured in osteogenic medium for 3 days and analyzed for DNA content, Annexin V/PI co-staining, and ALP Activity. Confocal imaging validated cellular uptake of the pBAE nanoparticles 24 h after transfection (Figure 2F). There was a significant decrease in DNA content following miR-29b transfection when compared to the non-transfected and scrambled controls as previously seen with the human osteosarcoma cells (Figure 2G). There was also a significant increase in the percentage of cells undergoing early apoptosis (Q2, $p = 0.03$) and a significant decrease in viable cells (Q4, $p = 0.04$) in K7M2 cells 3 days post miR-29b transfection when compared to the scrambled control (Figure S2C,D, Supporting Information). There was also no significant difference in ALP activity between the control and the miR-29b or Scramble groups, however, there was a significant decrease in ALP activity between the Scramble and the miR-29b groups.

To understand the mechanism by which miR-29b delivery induces selective apoptosis in the cancer cells, we treated SaOS2 cells with either miR-29b or Doxorubicin. We used Doxorubicin treatment as a positive control as Doxorubicin is well-established to induce intrinsic apoptosis[28] rather than extrinsic apoptosis (Figure S3A, Supporting Information). First studying the extrinsic apoptosis genes both miR-29b and chemotherapy treatment significantly downregulate *FADD* and *Caspase 8* expression compared to the untreated control (Figure S3B, Supporting Information). On the other hand when we study the intrinsic apoptotic genes both miR-29b and chemotherapy treatment follow similar trends, albeit slightly less significant with miR-29b treatment. Both miR-29b and chemotherapy significantly inhibit *BCL-2* expression (Figure S3B,C, Supporting Information) and upregulate *Bax* expression leading to a significant increase in the *Bax/BCL-2* ratio, a known marker of intrinsic apoptosis. This demonstrates that one potential mechanism in which miR-29b delivery induces apoptosis is by initiating the intrinsic apoptotic pathway.

2.3. Screening the Therapeutic Potential of miR-29b in a Controlled Predictive Model of the Disease

Recently, there has been increased interest in the use of 3D cultures to study the tumor microenvironment as they are more predictive of the in vivo situation.[7,29] With this in mind, osteosarcoma tumor spheroids containing a co-culture of both MSCs and osteosarcoma (SaOS2) cells were generated using a hydrogel microwell system[7] (**Figure 3**A). Following a 4 h transfection with pBAE nanoparticles (miR-29b, 20 nM), tumor spheroids were further cultured in osteogenic medium ± the FDA-approved chemotherapeutic Doxorubicin (1.8 μM, the 50% inhibitory concentration (IC_{50}) for SaOS2 cellsas previously determined[7]) for 7 days. Tumor spheroid growth was significantly hindered as evidenced by a significant decrease in DNA content regardless of transfection. In the absence of chemotherapeutics, miR-29b transfection led to a significant increase in DNA content (Figure 3B). Flow cytometry data revealed that this increase in DNA content was due to an increase in MSC proliferation or selective osteosarcoma cell apoptosis as the ratio of MSCs:SaOS2 cells tripled following transfection (Figure 3C). This was further verified in the H&E and Live/Dead staining with significant increase in extracellular matrix (ECM) production and positive dead

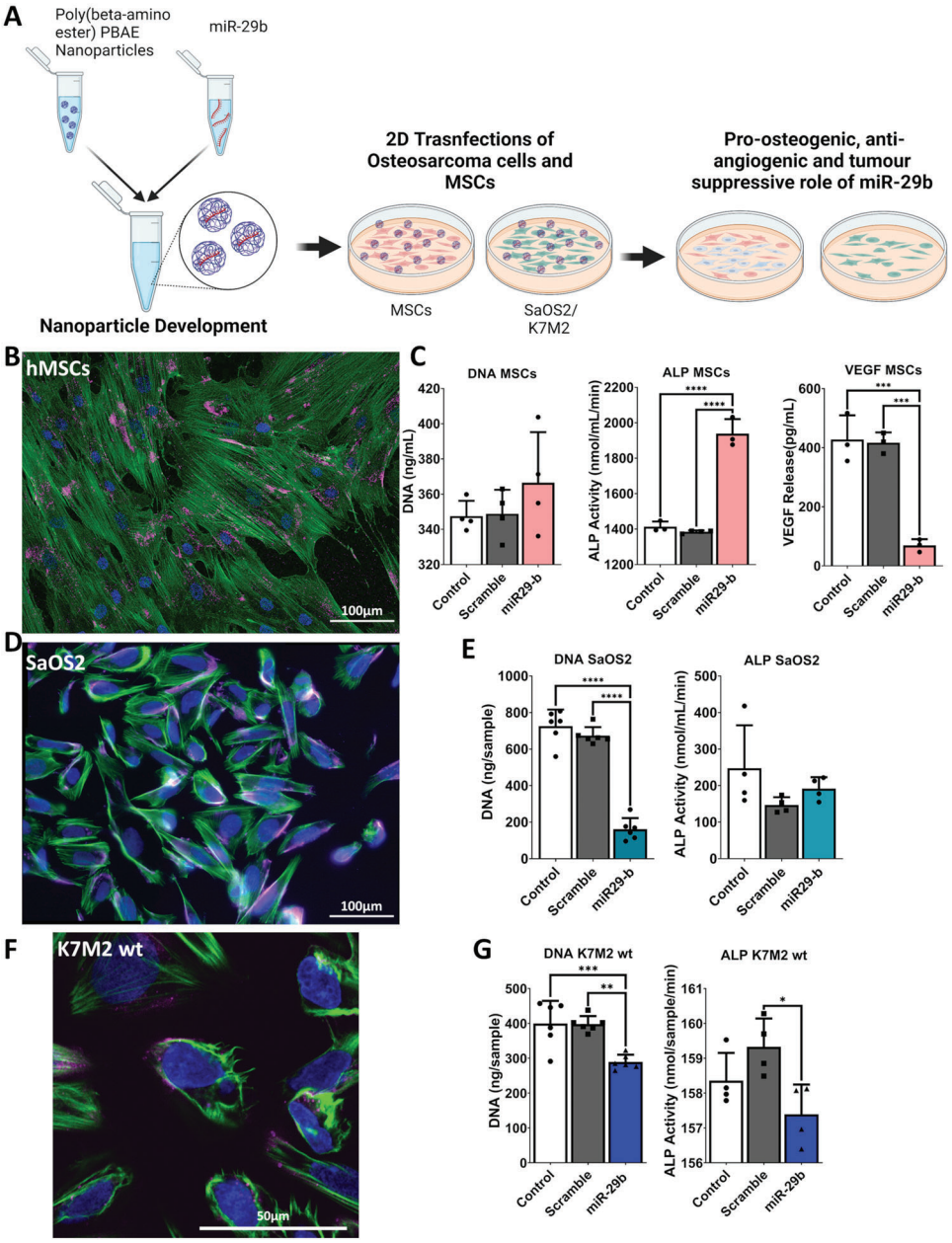

Figure 2. PBAE-nanoparticle-mediated transfection of human MSCs and osteosarcoma cells in 2D culture. A) Schematic of the experimental setup. Created with Biorender.com. B) Confocal images of human MSCs following 4 h transfection. C) DNA Content, ALP activity, and VEGF release over 7 days following transfection with miR-29b, or scramble-loaded pBAE nanoparticles. D) Confocal images of human osteosarcoma cells (SaOS2) following 4 h transfection with fluorescently labeled-pBAE nanoparticles. E) DNA Content and ALP activity over 3 days following transfection with miR-29b, or scrambled miR-loaded pBAE nanoparticles. F) Confocal images of Wild Type K7M2 mouse osteosarcoma cells following 4 h transfection. G) DNA Content and ALP activity over 3 days following transfection with miR-29b, or scramble-loaded PBAE nanoparticles. In all confocal images nuclei are stained in blue, actin-cytoskeleton in green, and miR-29b pBAE nanoparticles in pink. All data is represented as mean ± standard deviation (SD); $n = 4/6$. Statistical differences were assessed using one-way ANOVA. *p<0.05, **>0.01, ***$p < 0.001$, ****$p < 0.0001$.

staining present within the spheroids following miR-29b transfection (Figure 3D; Figure S4B, Supporting Information). The cytotoxic effect of the Doxorubicin on tumor progression was not hindered with the addition of miR-29b transfection, as evidenced by reduced tumor spheroid size and significant increase in dead staining present within the spheroids treated with Doxorubicin (Figure S4B, Supporting Information).

Finally, we investigated what effect miR-29b transfection was having at a gene level within our novel spheroid model. Looking at the prognostic genes for osteosarcoma, there is a clear anti-tumor effect when miR-29b was delivered to the tumor model. This effect was equivalent to the addition of Doxorubicin, as evidenced by the significant reduction in known prognostic markers *MMP2* and *MMP9*[30] mRNA expression in the miR-29b group

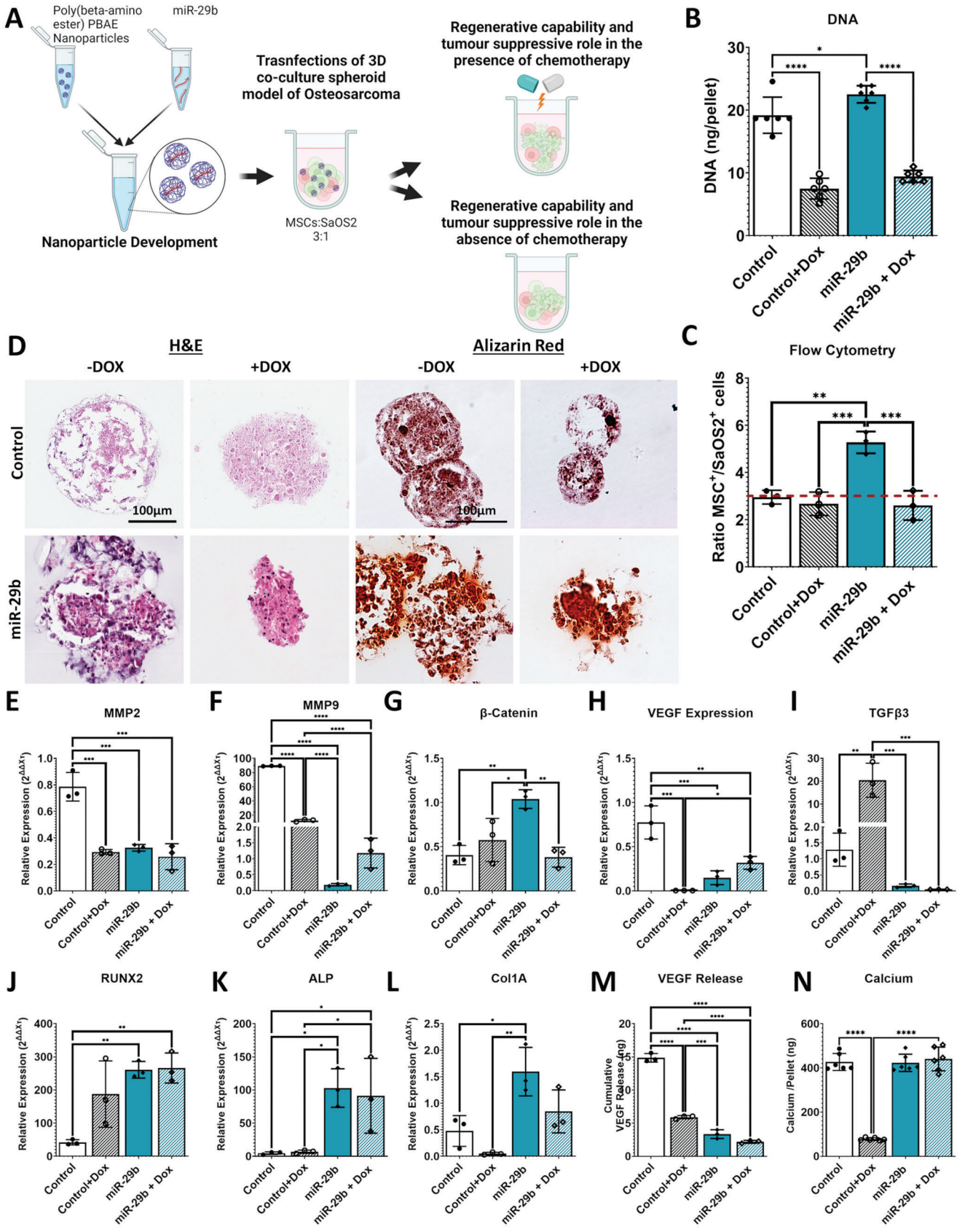

compared to the control (Figure 3E,F). Interestingly, there was a significant increase in β-Catenin mRNA expression when miR-29b was delivered alone (Figure 3G). As *β-Catenin* signaling also plays an important role in osteogenesis this increase in expression may be due to the increased osteogenic differentiation of the MSCs. MiR-29b delivery was seen to have an anti-angiogenic effect regardless of the addition of Doxorubicin. This was seen at both the gene (VEGF expression) and protein level (VEGF release) (Figure 3H,M). There was a significant decrease in TGF-β3 mRNA expression regardless of the addition of Doxorubicin when the spheroids were transfected with miR-29b. As studies have shown that one of the mechanisms behind miR-29b ability to induce osteoblast differentiation is by downregulating TGF-β3,[12] it validates the transfection efficiency of the pBAE nanoparticles to deliver the miR-29b even in a 3D environment (Figure 3I). Finally, as previously seen in our 2D in vitro culture studies, alizarin red staining revealed that miR-29b transfection led to a significant increase in mineralization in our tumor spheroids. This was apparent even when the tumor spheroids were also cultured in the presence of Doxorubicin (Figure 3D). This was further verified at both the gene level (*RUNX2, ALP, Col1A* mRNA expression) and protein level (calcium content) (Figure 3J–L,N), verifying miR-29b delivery promotes bone remodeling.

2.4. Development of the Hyaluronan-Based Injectable System for the Local and Sustained Release of pBAE:miR-29b Nanoparticles

After demonstrating the dual therapeutic role miR-29b delivery has in vitro, we tested its efficacy at suppressing tumor growth whilst simultaneously normalizing the dysregulation of bone homeostasis caused by both the chemotherapeutics and the osteosarcoma within the surrounding bone. An HA-based injectable system was developed to enable efficient, local, and sustained release of either the pBAE:miR-29b nanoparticles or BMP-2 (**Figure 4**A).

To form the HA-based hydrogel, HA primary amines were reacted with the 8-arm-PEG-NHS crosslinker containing a succinimidyl functional group, allowing for spontaneous hydrogel formation. The material properties revealed that the HA hydrogel was a soft hydrogel with a compressive modulus of 171.55 Pa ± 39.62 with a relatively low swelling ratio reaching an equilibrium swelling ratio of 1.3 (Figure S5A,B, Supporting Information). The gelation kinetics demonstrated that once the HA hydrogel and 8-arm-PEG-NHS crosslinker were mixed it took ≈1 min for gelation to begin (61 s) and a further 19 s for complete crosslinking to have occurred (Figure S5C, Supporting Information). Therefore, the crosslinking speed from start to finish of the hydrogel ≈1.2 min, thereby allowing for the delivery system to be easily injected using a standard 25G needle. In vitro release kinetics revealed that pBAE release from our HA delivery system followed two phases (Figure 4B). The first phase comprised of rapid release of ≈50% of the particles in the first 24 h, followed by a more sustained release reaching 100% after 15 days. The initial fast nanoparticle release is a result of the increased swelling occurring within the hydrogel, providing the first bolus release (Figure S5B, Supporting Information). This is followed by sustained release of the physically entrapped nanoparticles within the hydrogel upon hydrogel degradation, which is more gradual as we have previously demonstrated with other hydrogel delivery systems.[31] As HA-based hydrogels have been successfully tested as injectable carriers ofBMP-2,[32] which is widely known to induce bone remodeling[23] it was chosen as the control to evaluate the pro-osteogenic potential of our miR-29b:nanoparticles. In vitro release kinetics of the BMP-2 from the same delivery vehicle revealed a burst release of BMP-2 in the first three days with 42% of the overall concentration of growth factor released in this time frame (Figure 4C), over the next 33 days in culture there is a slow release of BMP-2 with only another 10–12% release of the total growth factor during this time.

To analyze the biological activity of the miR-29b pBAE nanoparticles post-release from the HA-based injectable system we prepared the HA hydrogel with and without miR-29b nanoparticles. We injected the hydrogels into a mold to create hydrogel disks and cultured them in PBS for 6 days in normoxic conditions (Figure S6A, Supporting Information). During this time we collected the conditioned medium and following 6 days of release analyzed the medium by fluorescence to calculate the concentration of nanoparticles within the medium (Figure S6B, Supporting Information). Once calculated we used this medium to treat either human MSCs (pro-osteogenic) or SaOS2 cells (pro-apoptotic) to evaluate the miR-29b biological activity after its release from the HA injectable system. Following 4 h of treatment with either conditioned medium taken from hydrogels (± miR-29b pBAE nanoparticles) or fresh miR-29b pBAE nanoparticles, the MSCs were further cultured for 7 days in expansion medium and analyzed for DNA content and ALP Activity. A similar response was seen in the MSCs treated with either fresh miR-29b pBAE nanoparticles or hydrogel plus miR-29b pBAE nanoparticles leading to a significant increase in ALP expression and MSCs proliferation compared to the untreated control (Figure S6C,D, Supporting Information). Interestingly, the HA hydrogel alone also led to an increase in MSC proliferation but no change in ALP activity.

To assess the biological activity of the miR-29b pBAE on osteosarcoma cells, human osteosarcoma cells (SaOS2) were treated with the conditioned medium taken from hydrogels (± miR-29b pBAE nanoparticles) or fresh miR-29b pBAE nanoparticles. Following a 4 h transfection period, the cells were cultured in expansion medium for 3 days and then analyzed for DNA content and ALP Activity. Similar to MSCs when treated

Figure 3. Spheroid growth, cancer progression, and mineralization following miR-29b transfection in the presence/absence of Doxorubicin using 3D tumor spheroid model of osteosarcoma. A) Schematic of the experimental setup. Created with Biorender.com. B) DNA content and C) analysis of the ratio of MSCs+ to SaOS2+ cells present within the spheroids. D) H&E and Alizarin Red staining of the tumor spheroids following 7 days post-transfection. Images taken at 20×. E–L) mRNA levels of *MMP2, MMP9, β-Catenin, VEGF, TGFβ3, RUNX2, ALP* and *Col1A* were analyzed by qRT-PCR. M) VEGF release and N) calcium content present within the tumor spheroids. All data were obtained following a 7-day culture period post-transfection and are represented as the mean ± SD; $n = 6$ (25 spheroids per experimental replicate) for biochemical assays; $n = 3$ (100 spheroids per experimental replicate) for PCR analysis. Statistical differences were assessed using one-way ANOVA with Tukey post-test. *$p < 0.04$, **$p < 0.007$, ***$p < 0.0005$, ****$p < 0.0001$.

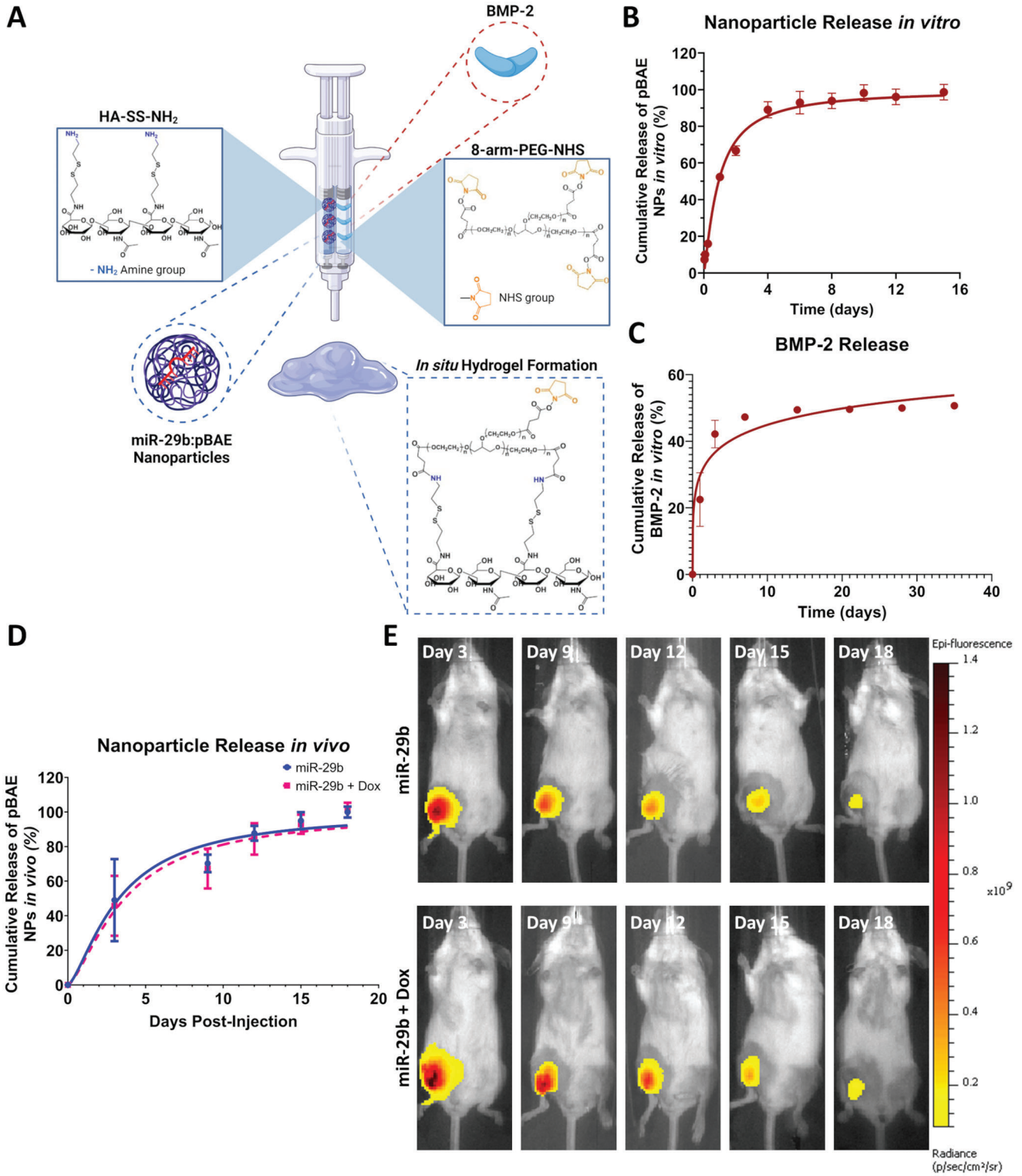

Figure 4. Development of a hyaluronan-based injectable system for the local and sustained release of pBAE nanoparticles or growth factors. A) HA-injectable hydrogel fabrication process: aqueous amine-modified HA (HA-SS-NH2) solution is crosslinked using the NHS-terminated 8-arm PEG crosslinker. The final chemical structure of the injectable HA hydrogel is found in the final scheme. Created with Biorender.com. B) Cumulative release of pBAE nanoparticles from HA hydrogel over 15 days in vitro. C) Cumulative release of BMP-2 from HA hydrogel over 35 days in vitro. D,E) Cumulative release of pBAE nanoparticles from HA hydrogel over 18 days following local administration of the HA hydrogel in orthotopic model for osteosarcoma. All data are represented as mean ± SD; $n = 4$ for in vitro release and $n = 8$ for in vivo release.

with a conditioned medium from the hydrogel alone, there was a significant increase in SaOS2 cell proliferation, however, this treatment also led to a significant increase in ALP activity in SaOS2 cells (Figure S6E,F, Supporting Information). The addition of miR-29b pBAE nanoparticles to the hydrogel did lead to a significant decrease in SaOS2 proliferation compared to the hydrogel alone however the pro-apoptotic effect was not as effective as the fresh miR-29b nanoparticles.

Finally, using our newly developed metastatic murine model for osteosarcoma (Figure S9, Supporting Information), we validated the injectability of our HA delivery system to non-invasively deliver the pBAE nanoparticles to the primary tumor site. The HA-based injectable system crosslinked in situ and allowed for local and sustained delivery of the miR-29b to the primary tumor site. Florescent IVIS imaging verified the in vitro release kinetics profile with ≈100% of the nanoparticles released from the HA hydrogel in ≈15–18 days post-implantation (Figure 4D). IVIS imaging also demonstrated that when locally administered there was focused delivery of miR-29b to the primary tumor site as evidenced by the accumulation of the nanoparticles around the tumor, with no downstream signal for any healthy organs (Figure 4E).

2.5. Localized miR-29b Delivery Supressed Tumor Growth Locally and When Combined with Systemic Doxorubicin Significantly Increased Survivability

Next, we assessed whether a combination therapy (systemic Doxorubicin and localized miR-29b) would suppress tumor growth compared to either therapy alone using an orthotopic model for osteosarcoma (**Figure 5**A). Systemic Doxorubicin of 2 mg kg^{-1} was administered intravenously twice a week over the course of 3 weeks and is equivalent to a dose of 6.5 mg m^{-2} given clinically.[33] Tumor size was measured by luminescence and vernier calipers twice a week for three weeks (Figure 5B,C). MiR-29b-treated mice (miR-29b, miR-29b + Dox) showed significantly slower tumor growth than all three controls (Figure 5B,C). When miR-29b was delivered along with systemic chemotherapy, compared to chemotherapy alone, our therapy provided a 45% reduction in tumor volume over 15 days. This corresponded to a significant increase in survival when compared to all three controls (Figure 5D). Specifically, when miR-29b was added to conventional chemotherapy there was an increase in 50% survival—from 24 days (chemotherapy alone) to 32 days (combination therapy). Furthermore, it was directly due to the miR-29b delivery and not the HA hydrogel, as the hydrogel alone group had no effect on tumor growth or survivability (Figure 5D).

2.6. Localized Delivery of miR-29b Significantly Reduced Osteolysis Caused by Chemotherapeutics and the Primary Tumor and Normalized Bone Homeostasis within the Surrounding Damaged Bone Following Two Weeks of Treatment

We sought to assess what effect if any the local delivery of miR-29b would have on the surrounding damaged bone. Our in vitro studies demonstrated the miR-29b delivery promoted bone remodeling by inhibiting TGF-β3 signaling thereby significantly increasing the expression for a panel of well-established osteogenic genes. Our in vivo study cooperated with these findings as μCT imaging, specifically around the primary tumor site (**Figure 6**B, red box), revealed a significant increase in bone volume when compared to systemic chemotherapeutic alone or untreated controls. Thereby, verifying that miR-29b delivery normalizes the bone homeostasis within the surrounding damaged bone by normalizing the dysregulation of bone lysis activity caused by the growing tumor. A similar trend was seen but without significance, in the same group when combined with systemic chemotherapeutics ($p = 0.066$). There was on average 75% reduction in osteolysis when miR-29b was delivered along with systemic chemotherapy, compared to chemotherapy alone. MicroCT 3D reconstructions and histological analyzes revealed the extent of the osteolysis due to the growing tumors in the untreated controls (No treatment, Hydrogel Alone) and clinical standard (Dox Alone, Figure 6C,D). In the untreated controls and clinical gold standard, it is clear that a sizable part of the tibia has been lysed away in place of tumor, due to the dysregulation of bone homeostasis caused by the tumor. Furthermore, there is little to no marrow cavity remaining in these groups (Figure 6D; denoted by M). On the other hand, both miR-29b treated groups (miR-29b and miR-29b + Dox) show slightly reduced tumor burden with enhanced bone tissue distribution complete with functional marrow cavities.

2.7. Systemic Doxorubicin and Localized miR-29b Delivery Significantly Reduced Osteolysis and Better Maintained Normal Bone Homeostasis in the Long-Term Compared to Local BMP-2 Delivery

To validate the clinical relevance of localized delivery of miR-29b to induce bone remodeling and normalize bone homeostasis, the therapeutic potential was directly compared to BMP-2 delivery, which is widely known to induce bone remodeling.[23] A concentration of 5 μg of BMP-2,[34] was loaded into the HA-based injectable delivery system and following the 14-day inoculation period was non-invasively injected around the primary tumor site. MicroCT analysis was used to visualize and quantify bone formation around the primary tumor site pre-treatment (which corresponds to 2 weeks after tumor induction), 2- and 4 weeks post-treatment (which corresponds to 4 and 6 weeks after tumor induction respectively). There was a trend toward increased bone formation in both the BMP-2 and miR-29b groups ($p = 0.5$) compared to their counterparts with combined systemic chemotherapeutics (BMP-2 + Dox, miR-29b + Dox) 2-weeks post-treatment (**Figure 7**B). MicroCT 3D reconstructions reveal that this increase in bone volume is due to the presence of ectopic bone formation surrounding the tibia. This was not present in the miR-29b + Dox group (Figure 7D). Interestingly, there was more ectopic bone formation observed surrounding the tibia (denoted by red arrows) in the BMP-2 group when compared to the BMP-2 + Dox group even though both groups received the same hydrogel with the same concentration of BMP-2, the only difference was the addition of systemic Doxorubicin.

Despite the small number of animals which survived to the 4-week timepoint ($n = 4$ per group), a clear effect of the combination therapy on osteolysis was observed. There was an increase in

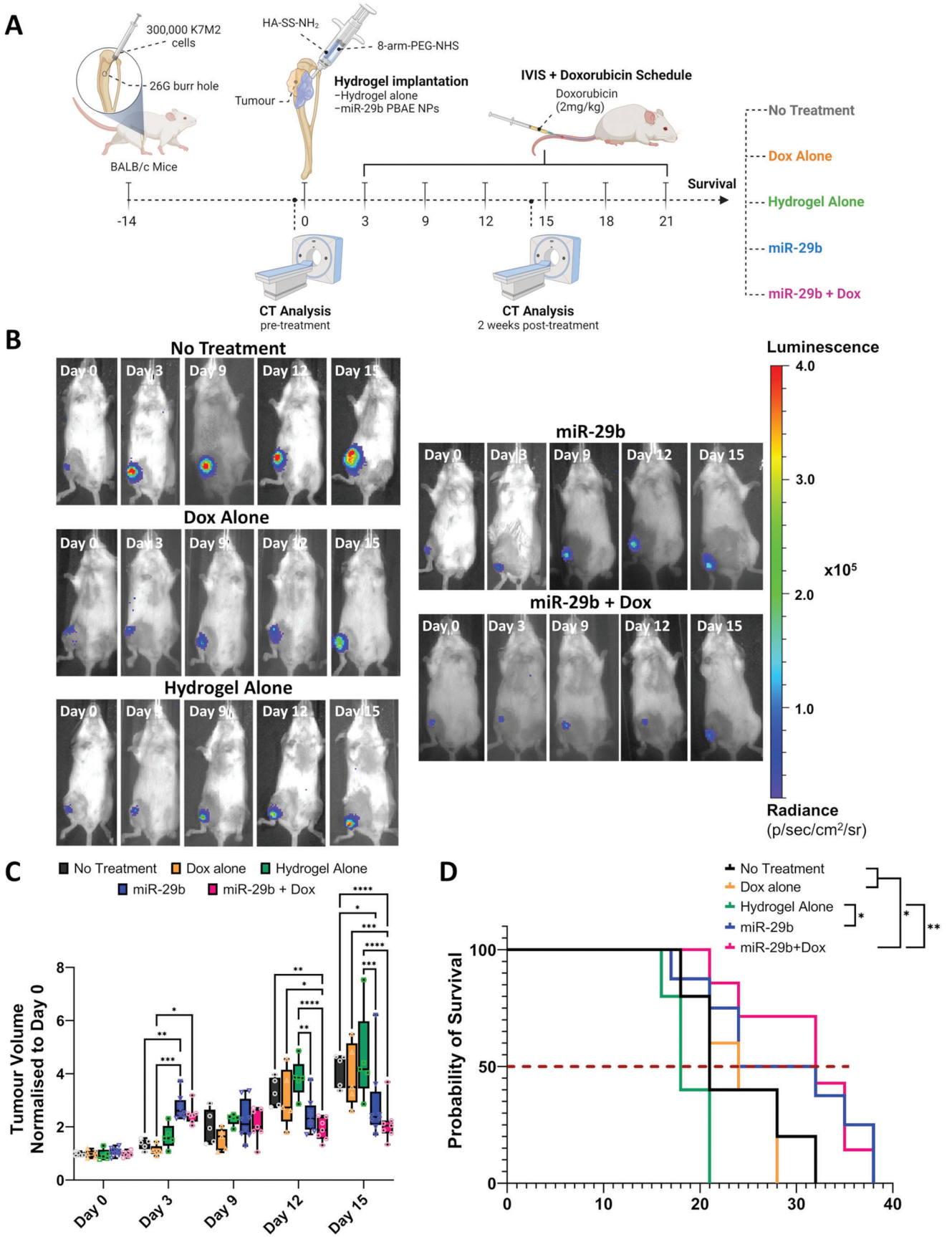

osteolysis (measured by percentage change in bone volume/total volume (BV/TV)) in both the BMP-2 and miR-29b groups from 2 to 4 weeks post-treatment (Figure 7C). In contrast, bone homeostasis was maintained in the BMP-2 + Dox and the miR-29b + Dox groups as bone volume remained the same in the BMP-2 + Dox group, while there was a significant increase in bone formation as bone volume was significantly increased from 2- to 4-weeks post-treatment in the miR-29b + Dox group. This was further verified in the 3D reconstructions and histological analyzes (Figure 7D,E). A significant amount of ectopic bone formation was present even 4 weeks post-treatment in the BMP-2 group. MicroCT reconstructions showed little change to the cortical bone in the BMP-2 group but histological analysis revealed little to no trabecular bone present within the cortical shell due to tumor growth. The overall bone distribution was better maintained in the miR-29b group compared to the BMP-2 group, as both cortical and trabecular bone were still present. A similar trend was seen in the corresponding groups with combined systemic chemotherapeutics (BMP-2 + Dox, miR-29b + Dox). Looking at the bone architecture we can see a small amount of ectopic bone formation with only the cortical shell remaining in the BMP-2 + Dox group. Conversely in the miR-29b + Dox group superior bone distribution and architecture are observed in both the cortical and trabecular bone (Figure 7E).

3. Discussion

Despite the distinct clinical need for more effective treatment options, there have been no major improvements in the treatment of osteosarcoma since the 1970s.[3] Furthermore, as osteosarcoma is such an aggressive disease, the surgical intervention usually involves total reconstructions of the limbs or in most cases amputation, despite this, most of the research to date has focused on the prevention of metastases, with little attention to bone repair or salvation. This study introduces for the first time the therapeutic potential of miR-29b in inhibiting osteosarcoma tumor growth as well as the immense potential of pBAE nanoparticles as a therapeutic delivery vehicle to treat osteosarcoma when delivered locally over time via an injectable adhesive hydrogel. Furthermore, our study outlines a truly novel combination therapy —systemic chemotherapy and localized miR-29b— to enhance the therapeutic potential of chemotherapy whilst simultaneously providing the surrounding damaged bone the necessary cues for bone formation. The HA-based injectable delivery system crosslinked in situ in a matter of minutes and allowed for local and sustained delivery of the miR-29b to the primary tumor site. The clinical translation of the hydrogel would allow clinicians to inject directly into the defect site during tumor resection, as no UV or temperature is needed for cross-linking. Therefore, this localized therapy has the potential to be integrated into the current clinical treatment regimen as a potential add-on to conventional chemotherapy to further improve clinical outcomes.

In the oncology field,miRNAs and their role in regulating cancer progression have been a revolutionary discovery over the last decade.[35] Yet, there have only been 15 papers published since 2010 on miRNA delivery for the treatment of osteosarcoma.[36] Herein, we developed a pBAE nanoparticle delivery vector and tested its ability to efficiently deliver miR-29b to human and murine osteosarcoma cancer cells and surrounding healthy stromal cells in vitro in both 2D and 3D cultures. Specifically, we demonstrated that the pBAE nanoparticles were significantly more effective at delivering miRNA to osteosarcoma cells than commercially available transfection reagent Lipofectamine (Figure S9, Supporting Information). This increase in transfection efficiency is due to the cationic nature of the nanoparticles, which enables them to condense the negatively-charged miRNA more efficiently than other polymeric-based nanoparticles.[26,37] Additionally, the cationic surface density (5.6 mV ± 3.5) of pBAE nanoparticles also allowed for efficient cell internalization which improved their endosomal escape due to the proton sponge effect. Furthermore, the pBAE backbone polymer contains ternary amine groups which act as a buffer in the low pH environment of endosomes, which further leads to its disruption, and release of the encapsulated miRNA, resulting in more efficient delivery than liposomal-mediated transfection.[26,37] As pBAE nanoparticles have never been studied in the context of osteosarcoma this vital information will be critical in the design of future gene delivery options for osteosarcoma patients.

One of the major limitations that impede the advancement of miRNA therapy, is due to low delivery efficiency as a result of poor penetration of miRNAs into the tumor tissues. Therefore, we assess the penetrability of the pBAE particles by analyzing their potential to deliver the miR-29b within a 3D spheroid model of osteosarcoma.[7] The 3D spheroid model allowed for spatial arrangement of the two cell types (MSCs, SaOS2) with enhanced cell-to-cell contact and the ability to form proliferative gradients, hypoxia, and necrosis.[7,38] Furthermore, as certain ECM components were found to be expressed at high levels in 3D spheroids, the model could effectively mimic the penetration barriers seen in vivo, thereby allowing us to study the penetration, distribution, and uptake of the nanoparticles within these models.[38–39] Previous studies have suggested that nanoparticles that are capable of diffusing through pores between the collagen fibrils, measured between 20–40 nm, are needed to penetrate compact tumors, or between 75–130 nm in size when penetrating poorly organized tumors.[38,40] Yet, despite their larger size (151 nm), our pBAE nanoparticles were capable of penetrating our tumor spheroids (≈0.28 mm in diameter[7]) after only 4 h of transfection, resulting in measurable changes at the genomic level within the two cells types (Figure 2). This increase

Figure 5. Localized miR-29b delivery suppressed tumor growth locally and when combined with systemic Doxorubicin significantly increased survivability. A) Schematic of the developed metastatic orthotopic osteosarcoma mouse model including all the treatment groups. Created with Biorender.com. B) Live imaging (IVIS) following inoculation with K7M2-Luc labeled osteosarcoma cells. C) Quantitative evaluation of tumor size calculated using the following formulae (Width^2 × Length)/2 at different time points. All data were obtained over 15 days following the various treatment regimens and are represented as mean ± SD (n = 5/8 per group). Statistical differences were assessed using two-way ANOVA with a Tukey post-test. *$p < 0.01$, **$p < 0.006$, ***$p < 0.0008$, ****$p < 0.0001$. D) Kaplan–Meier survival curves of mice treated with the indicated formulation using a 1000 mm^3 tumor volume or poor body condition as the endpoint criterion. Statistical analysis was performed using a log-rank Mantel–Cox test. *$p < 0.02$, **$p < 0.0018$. The red dashed line denotes a 50% survival rate.

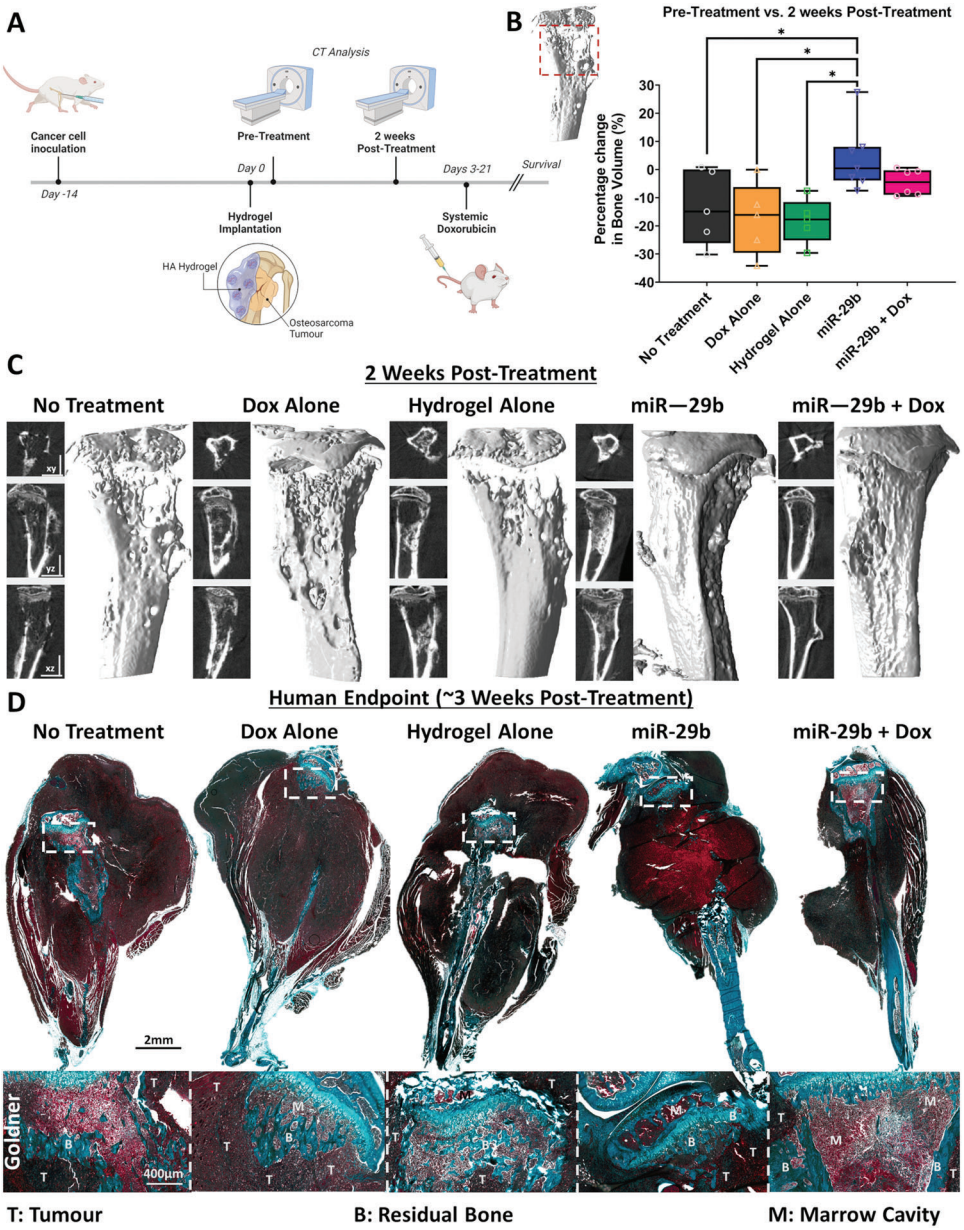

Figure 6. miR-29b delivery significantly reduced osteolysis due to tumor burden and led to an increase in bone volume after 2 weeks of treatment. A) Schematic of the timeline for μCT analysis to assess osteolysis following treatment with miR-29b:nanoparticles. Created with Biorender.com. B) Percentage change in bone volume pre versus post-treatment. All data are represented as mean ± SD; $n = 5/8$. Statistical differences were assessed using a one-way ANOVA with a Tukey post-test. *$p < 0.01$. C) 3D reconstructions and X-rays images in the *xy, yz, zx* planes of the worst healers of the μCT data for each group at following 2 weeks of treatment. D) Representative Goldner's Trichrome-stained sections from all the experimental groups which mice all had a similar endpoint (≈3 weeks post-treatment). Images were taken at 20×. B denotes remaining bone tissue, M denotes marrow, and T denotes tumor.

in penetration may also be attributed to the cationic nature of the pBAE nanoparticles. Previously, studies have shown that cationic nanoparticles are significantly more effective in tumor growth inhibition than their anionic or neutral counterparts in a variety of tumor models due to improved permeability and penetration capabilities.[41] Furthermore, as the current process for testing the effectiveness of nanoparticles relies greatly on animal models, our unique spheroid system provides useful insights into the effectiveness of the pBAE nanoparticles in delivering the miR-29b within the tumor microenvironment before conducting a full pre-clinical in vivo study.

Dysfunction of miRNAs is often associated with tumor formation and progression as manipulation of the oncogenic pathways can influence tumor progression.[16] Specifically, studies have shown that miR-29b was significantly downregulated in osteosarcoma tissues.[42] Previous in vitro studies have shown that miR-29b delivery to osteosarcoma cells suppresses proliferation and migration and induces cell apoptosis of osteosarcoma cells;[14]

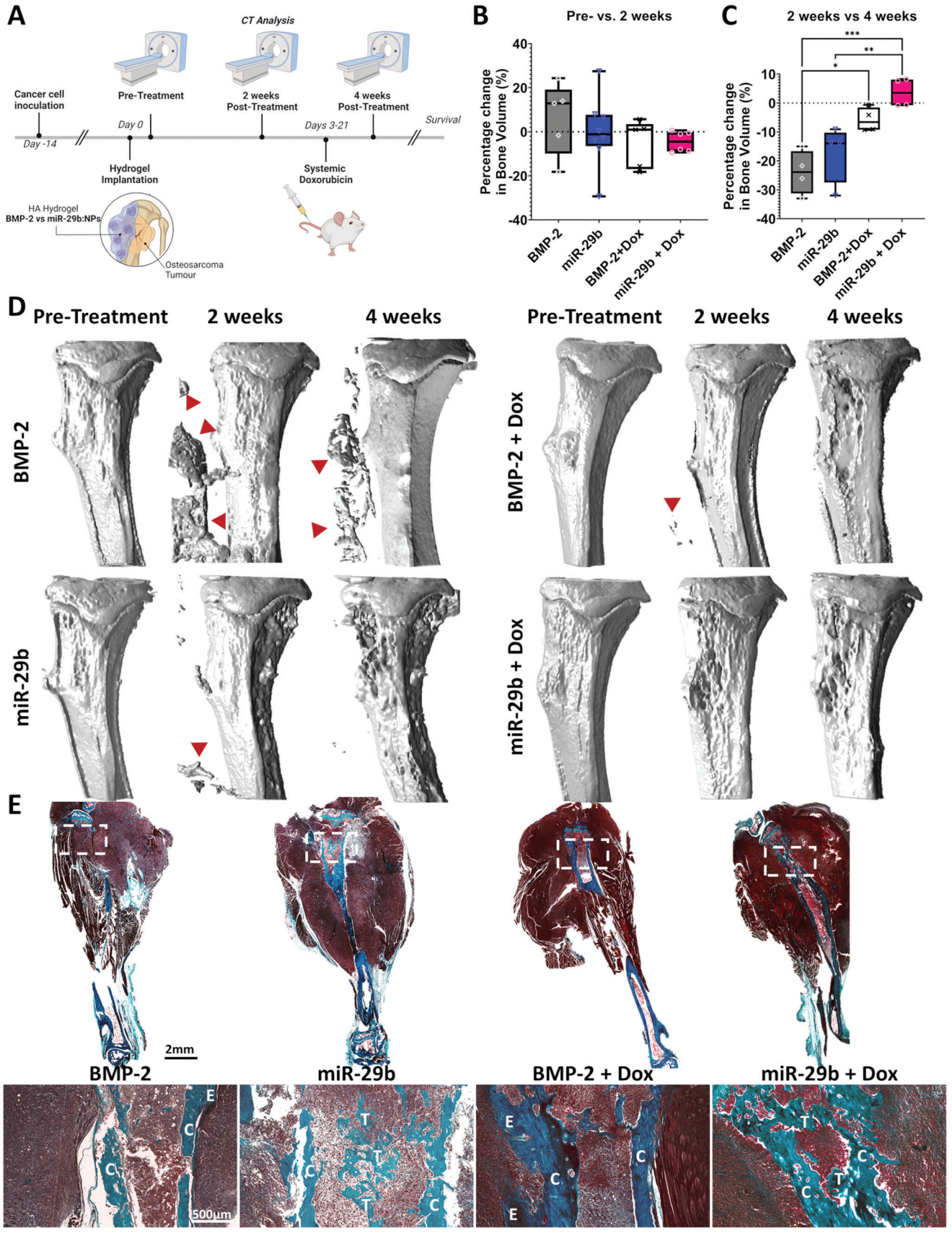

however, the mechanism by which miR-29b induces apoptosis in osteosarcoma cells remains unclear. Our current study establishes that the delivery of miR-29b to the osteosarcoma cells, where miR-29b is down-regulated or silenced, induces the intrinsic apoptotic pathway (Figure S3, Supporting Information) as previously seen when delivered to other cancer cells,[10b,d,e,11] but not in the context of osteosarcoma. It is well documented that miR-29b-3p targets BCL-2 modifying factor (BMF)[43] and acts as a proapoptotic factor that binds to the 3′-UTR of BMF. We hypothesize that when miR-29b-3p is delivered to osteosarcoma cells where miR-29b was not overexpressed, it inhibits BMF expression which in turn inhibits BCL-2 expression inducing intrinsic apoptosis within these cells. Interestingly, when miR-29b is delivered to healthy cells, where its expression is normal, it led to an overexpression of miR-29b, which had a pro-osteogenic effect on the cells. When miR-29b was delivered to the surrounding healthy stromal cells, it induced cell proliferation and promoted the pro-osteogenic effect (Figures 2 and 3).[44] There are many studies that have characterized the role miR-29b plays in relation to tumorigenesis,[10] but only a few studies which have examined its role in osteogenesis.[12a,44,45] Specifically, studies have shown that miR-29b is a positive regulator of osteoblast differentiation by down-regulating inhibitory factors of osteogenic signaling pathways and controlling expression of collagen in differentiated osteoblasts.[12a] Our current study follows from this by delineating the network of genes regulated by miR-29b and demonstrating how this stimulatory effect is unaffected by the addition of chemotherapeutics. Taken together, our study confirms the dual therapeutic role of miR-29b delivery by enabling selective cancer-cell killing while simultaneously promoting osteogenesis in the surrounding healthy tissues.

Finally, in an orthotopic metastasis model for osteosarcoma, we demonstrated the antitumor efficacy of localized delivery of pBAE:miR-29b complexes using an HA-based injectable delivery system. This therapeutic effect has previously only been shown in prostate and cervical cancer,[10b,22] never in osteosarcoma. Moreover, delivery of the combined therapy (systemic Doxorubicin and localized miR-29b) further improved preclinical outcomes, leading to a significant increase in 50% survival from 24 days to 32 days when compared to the current clinical gold standard of systemic chemotherapeutics. This validates the plausibility of introducing our novel localized miRNA therapy as a potential add-on to conventional chemotherapy.

Yet, despite the promising results in reducing the tumor burden locally, none of the animals were fully cured. This may in part be attributed to the clinically relevant orthotopic model used in this study. Over the last 5 years, there are over 20 journal articles[46] investigating the divergent relationship between osteosarcoma elimination and bone regeneration, yet none of these studies evaluated the dual-therapeutic potential of their therapy in an orthotopic model. Instead, they utilize two different in vivo models, a subcutaneous osteosarcoma tumor model (rather than an orthotopic model), and a separate segmental bone defect model in a healthy animal. Despite the fact that osteosarcoma has been shown to manipulate the physiological bone remodeling process[47] so analyzing its ability to regenerate bone in a healthy animal is not a true representation of what would happen if applied in the clinic. Only one research group has come close by utilizing a tumor plague embedment method.[48] Yet, this method still utilized a subcutaneous tumor model which does not take into account the proper interactions between the tumor cells and their normal bone/muscle/cartilaginous microenvironment. This study is the first to evaluate the dual-therapeutic effect in a clinically relevant orthotopic model for osteosarcoma.

Another mitigating factor may be the dosing regimen used in this study. Only one dose of miR-29b was administered and although there was a therapeutic response in the 15 days in which the nanoparticles were being released, this did not lead to full tumor elimination. Future studies aim to evaluate if a second dose of miR-29b after 15 days may significantly increase its therapeutic potential and prevent metastases. Furthermore, the interaction of tumors and host immune systems has long been recognized to be a critical aspect of tumor survival in malignancies. Despite this, the relationship between tumor and host immune microenvironment, their interactions, and opportunities for exploitation of immune-mediated therapies remain poorly defined in osteosarcoma.[49] Previous studies have shown that chemotherapeutics like cisplatin and Doxorubicin, have the capacity to upregulate programmed death-ligand1 (PD-L1) expression on cancer cells and which in turn promotes antitumor immunogenicity, via activation of cytotoxic T cells.[50] We have also previously shown in our lab that delivery of a Stimulator of Interferon Genes (STING) agonist is effective therapy at eliminating melanoma.[51] As metastasis was not the focus of this study, we did not investigate any further combination therapies but future studies will evaluate the synergistic potential of a triple therapy of combining localized nanoparticle-mediated gene delivery with systemic chemotherapy and immunotherapies like anti-PD1 or STING.

Finally, although chemotherapy is effective in controlling cancer cell growth, it has also been shown clinically to disrupt bone homeostasis,[6] resulting in a dysregulated bone lysis activity significantly hindering the surrounding bone's ability to regenerate following surgical intervention. Previously, we suggested that BMP-2 delivery may not be an effective therapy to aid with the regenerative capability of the damaged bone caused by excising the tumor while the patient is undergoing chemotherapy.[7] Our study further corroborates these findings as when BMP-2 is delivered alone, ectopic bone formation is found surrounding the tibia, but when the same hydrogel loaded with the same

Figure 7. Localized delivery of miR-29b significantly reduced osteolysis and led to enhanced bone tissue distribution compared to clinical gold standard BMP-2 delivery even in the presence of chemotherapeutics. A) Schematic of the timeline for μCT analysis to assess osteolysis following treatment with miR-29b:nanoparticles versus BMP-2 delivery. Created with Biorender.com. B,C) Percentage change in bone volume pre- versus 2 weeks post-treatment (B) and 2 weeks versus 4 weeks post-treatment (C) for all four treatment groups. All data is represented as mean ± SD; $n = 5/8$ (pre and 2-week post-treatment), $n = 4$ (4 weeks post-treatment). Statistical differences were assessed using a one-way ANOVA with a Tukey post-test. *$p < 0.01$, **$p<0.004$, ***<0.0007. D) 3D reconstructed in vivo μCT analysis of the mouse tibias over the 4 weeks of treatment. The red arrowheads denote ectopic bone. E) Representative Goldner's Trichrome-stained sections from all the experimental groups which mice all had a similar endpoint. Images were taken at 20×. C denotes remaining cortical bone, T denotes remaining trabecular bone, E denotes ectopic bone formation.

concentration of BMP-2 was delivered and combined with systemic chemotherapeutics the stimulatory effect was significantly diminished (Figure 7). Furthermore, the long-term effect on bone homeostasis induced by the osteolytic tumor cannot be overcome by miR-29b or BMP-2 alone as both groups saw a significant decrease in bone volume from 2 to 4 weeks post-treatment. It was only when combined with systemic Doxorubicin that there was a significant decrease in the osteolysis caused by the tumor by decreasing the tumor burden in these groups. However, it is clear that both chemotherapy and the tumor itself can significantly hinder bone's ability to regenerate,[6c,d,52] and that this effect cannot be overcome by standard osteogenic growth factors. Interestingly, similar to what we demonstrated using our spheroid model, the long-term effect of the combined therapy (systemic Doxorubicin and localized miR-29b) significantly reduced osteolysis due to decreased tumor burden and maintained bone architecture with little to no ectopic bone formation, even in the presence of chemotherapeutics. This study demonstrates for the first time the immense potential of miRNA delivery for normalizing bone homeostasis, as its pro-osteogenic effect is in no way hindered by the addition of chemotherapeutics, unlike BMP-2 delivery. This may be due to the fact that growth factors regulate an abundance of miRNAs, and by delivering specific miRNAs, one can deliver the necessary cues directly to the cells, without being affected by off-target toxic effects induced by the chemotherapeutics. This anti-cancer and pro-osteogenic effect of miR-29b delivery may extend to other types of cancer. In multiple myeloma, for example, elevated osteoclast activity together with impaired osteoblast function is commonly triggered by tumor cells that proliferate in the bone marrow.[12b] Our miR-29b:pBAE nanoparticles could potentially be delivered to not only treat the tumor cells but also repair osteoblast function. Furthermore, as bone is one of the most common locations of cancer cell metastasis, any therapeutic that inhibits bone tumor growth whilst simultaneously aiding in bone regeneration which the patient is undergoing chemotherapy would significantly benefit not only osteosarcoma patients but any cancer patients with bone metastases (breast, lung, lymphoma, myeloma, prostate, and thyroid).[53]

Taken together, this study introduces the therapeutic potential of localized nanoparticle-mediated miR-29b delivery in suppressing osteosarcoma growth whilst simultaneously providing the surrounding damaged bone the cues needed to normalize the dysregulation of bone homeostasis caused by tumor growth. A smart delivery vehicle was developed to enable targeted, efficient, local, and sustained delivery of miRNAs or growth factors, which can easily be integrated when excising the tumor as a potential add-on to conventional chemotherapy. This novel combined therapy could further improve clinical outcomes by significantly reducing primary tumor mass and providing vital information that can inform the design of future combination therapies for these young patients.

4. Experimental Section

Cell Culture: Human osteosarcoma cell line (SaOS2, HTB-85) and human mesenchymal stromal cells (MSCs, PCS-500-012) were commercially purchased from ATCC. K7 murine osteosarcoma cell line (K7M2-WT, CRL-2836) isolated from the proximal tibia of a BALB/c mouse was commercially purchased from ATCC. Expansion of all cell types was conducted in normoxic conditions and Expansion Medium [Dulbecco's modified Eagle medium (DMEM; Biosciences) supplemented with 10% fetal bovine serum (FBS, Gibco), 1% penicillin (100 U mL^{-1}) and 1% streptomycin (100 µg mL^{-1}) (Biosciences)], was changed twice weekly. Human MSCs and osteosarcoma cells were used at the end of passage 5 for in vitro analysis and murine osteosarcoma cells were used at the end of passage 7 for in vivo inoculation.

Synthesis of Poly-beta-amino-esters (pBAE) Polymers: Synthesis of pBAEs was performed via a two-step procedure, as previously described.[24] First, C6 acrylate-terminated polymer was obtained by the addition reaction of 5-amino-1-pentanol (0.426 g, 4.1 mmol) and hexylamine (0.422 g, 4.1 mmol) to 1,4-butanediol diacrylate (2.0 g, 9.1 mmol). The reaction was carried out at 90 °C for 24 h. Second, C6 polymer was end-capped with thiol-terminated arginine peptide (Cys–Arg–Arg–Arg) at a 1:2.1 molar ratio in dimethyl sulfoxide (DMSO) in an overnight, room temperature reaction. The resulting polymer was purified and collected by precipitation in a mixture of diethyl ether and acetone (7:3). pBAE polymer structure was confirmed by ^{1}H-NMR (400 MHz Varian (NMR Instruments, Clarendon Hills, IL, USA)). Polymerization was previously confirmed by HPLC-SEC, and the resulting polymer had a weight-average molecular weight of 2500 g mol^{-1} (relative to polystyrene standards) and a polydispersity (M_w/M_n) of 1.81, showing a relatively broad statistical distribution of polymer chain lengths.

miR-29b-pBAE-Nanoparticle Formation and Characterization: MiR-29b:pBAE nanoparticles were performed by mixing equal volumes of pBAEs polymer and miR-29b in 12.5 mM acetate buffer (AcONa) at their appropriate concentration. Briefly, pBAE stock solutions in DMSO (100 mg mL^{-1}) were diluted in 12.5 mM AcONa at appropriate concentrations to obtain the desired pBAE:miR-29b weight/weight ratio. The pBAE polymer was added to a solution of miR-29b, incubated at room temperature for at least 5 min, and precipitated in two volumes of PBS 1×. The nanoparticles were purified by centrifugal filtration (10 kDa MWCO Amicon Ultra-4 mL Centrifugal Filters, Millipore), and filtered through a sterile 0.22 µm membrane. The resulting nanoparticles were characterized by an agarose retardation assay and dynamic light scattering (DLS). To assess miR-29b retardation, different miR-29b-to-pBAE (Horizon Discovery, miRIDIAN microRNA Human hsa-miR-29b-3p – Mimic) ratios (w/w) between 10 and 400 were studied. pBAE:miR-29b complexes were freshly prepared and loaded in 2% E-Gel Precast Agarose Gels (Thermo Fisher), run following the manufacturer's instructions, and visualized in fluorescence mode. Biophysical characterization of nanoparticles was performed using a ZetaSizer Nano ZS equipped with a He–Ne laser (λ 1/4 633 nM) at a scattering angle of 137° (Malvern Instruments Ltd., Malvern, UK). Hydrodynamic diameter (nm), PDI, and surface charge of nanoparticles were measured.

Cellular Uptake and Transfection Efficiency: To determine the optimum concentration of pBAE nanoparticles and culture conditions for transfection, human MSCs were seeded onto 24 well plates with polymer coverslip (Corning, P24-1.5P) at a seeding density of 2.6×10^4 cells cm^{-3}. pBAE:miRNA complexes were performed at a concentration of 100:1 miR29-b:pBAE ratio. After seeding, MSCs were transfected with 10 nM, 20 nM, or no pBAE nanoparticles loaded with (fresh expansion media) for 4 h. Following transfection cells were either fixed overnight in 4% paraformaldehyde for confocal imaging, or fresh media was applied (either expansion medium or osteogenic medium [expansion medium + 100 nM dexamethasone, 50 mg mL^{-1} ascorbic acid, and 10 mM β-glycerol phosphate; all Sigma-Aldrich]) and cultured for a further 7 days. After 7 days of culture, ALP expression into the media was used as a measure of transfection efficiency. This was measured using a colorimetric assay of enzyme activity (SIGMAFAST p-NPP Kit; Sigma Aldrich), which uses p-nitrophenyl phosphate (pNPP) as a phosphatase substrate with ALP enzyme (Sigma Aldrich) as a standard[54].

To validate the transfection efficiency of the pBAE nanoparticles the transfection potential was directly compared to the commercially available transfection reagent Lipofectamine (RNAiMAX, Thermofisher). Briefly, human MSCs were seeded at 2×10^4 cells cm^{-2} in a standard 24-well plate. After seeding MSCs were transfected with 20 nM of either pBAE:miR-29b

complexes for 4 h or 20 nM Lipfactamine:miR-29b complexes for 24 h. Following transfection fresh media was applied (either expansion medium or osteogenic medium) and cultured for a further 7 days. ALP activity was measured after 7 days of culture.

To validate the pro-osteogenic, anti-angiogenic potential of miR-29b delivery, human MSCs were seeded at 2×10^4 cells cm^{-2} in a standard 24-well plate. Following seeding MSCs were transfected with 20 nM of either pBAE:miR-29b (miR-29b) complexes or pBAE:siRNA (Scramble) complexes (Qiagen, AllStars Negative Control siRNA) or cultured in standard control medium (control) for 4 h. Following transfection fresh osteogenic media was applied and the cells were cultured for a further 7 days. ALP expression was measured after 7 days of culture. An enzyme-linked immunosorbent assay was used to quantify the levels of VEGF (Bio-Techne, MN, USA) released by the cells. The cell culture media was analyzed following 7 days of culture. Assays were carried out as per the manufacturer's protocol and analyzed on a microplate reader at a wavelength of 450 nM as previously described.[7,34a,55] To assess DNA content, cells were subjected to cell lysis by three cycles of freeze–thawing in molecular-grade water.[56] DNA content was measured using Quant-iT PicoGreen dsDNA Assay (BD Biosciences), with calf thymus DNA as a standard as previously described.[7,57]

To validate the apoptotic nature of miR-29b delivery to cancer cells human osteosarcoma cells (SaOS2) and mouse osteosarcoma cells (K7M2) were seeded onto 24 well plates with polymer coverslip (Corning, P24-1.5P) at a seeding density of 2×10^4 cells cm^{-3}. pBAE:miR-29b (miR-29b) and pBAE:siRNA (Scramble) complexes were prepared as mentioned above and following seeding both cell types were transfected with 20 nM of either complex or cultured in osteogenic medium (control) for 4 h. After transfection, cells were either fixed overnight in 4% paraformaldehyde for confocal imaging, or fresh media was applied and cultured for a further 3 days. ALP expression into the media was assessed after 3 days of culture. DNA content was also measured as mentioned above following 3 days of culture.

Flow Cytometry—Annexin V/PI Co-Staining: Human MSCs, SaOS2 cells, and K7M2 cells were seeded in a 24-well plate as described above. Following seeding cells were with 20 nM of either pBAE:miR-29b (miR-29b) complexes or pBAE:siRNA (Scramble) complexes (Qiagen, AllStars Negative Control siRNA) or cultured in standard control medium for 4 h. Following transfection fresh medium was applied to the transfected groups and 1.8 µM of Doxorubicin (IC_{50} concentration previously determined[7]) was added to the media of the non-transfected group as a positive control. Cells were further cultured for 3 days before Annexin V-PI double staining was performed following the manufacturer's protocol (640919, BioLegend, London, UK). Briefly, cells were washed twice with cold BioLegend's Cell Staining Buffer, and then resuspend cells in Annexin V Binding Buffer at a concentration of 1.0×10^6 cells mL^{-1}. Transferred 100 µL of the cell suspension to the 5 mL tube and added 5 µL of APC Annexin V and 10 µL of PI solution. Vortexed and incubated for 15 min at room temperature in the dark before adding 400 of Annexin V Binding Buffer to each tube. The cell suspensions were analyzed by flow cytometry using a BD LSR II HTS-1 flow cytometer (BD Biosciences) to determine apoptosis. All data were analyzed using Flowjo software (Flowjo LLC), gating strategy could be found in Figure S7 (Supporting Information).

Osteosarcoma Spheroid Model: Microwells were created using a molding system as previously described[7,58] (Figure S4A, Supporting Information). Briefly, sterile molten agarose solution (4% w/v) was pipetted into a well of a 6-well plate, where custom-made 3D printed positive molds were inserted. Once cooled, the positive mold was pulled from the agarose, leaving 401 microwells within each well. All agarose microwells were soaked overnight in DMEM prior to cell seeding. A 3:1 seeding ratio of human MSCs to osteosarcoma cells (MSC:SaOS2) was used as previously described.[7] Cells were seeded into the microwells by pipetting an appropriate density (4000 cells per microwell) into each well. After seeding, plates were centrifuged at 700 × g for 5 min to collect cells at the bottom of each well. Plates were then incubated in an expansion medium for 72 h to allow for formation of tumor spheroids. pBAE:miR-29b nanoparticles were prepared as mentioned above and the osteosarcoma tumor spheroids were either transfected with 20 nM concentration of pBAE nanoparticles for 4 h or cultured in an expansion medium for 4 h. Following transfection fresh media was applied and the tumor spheroids were cultured under the following culture conditions for a further 7 days of culture: 1] Control: cultured in osteogenic medium without transfection; 2] Control + Dox – cultured in osteogenic medium plus 1.8 µM of Doxorubicin (IC_{50} concentration previously determined[7]) without transfection; 3] miR-29b: cultured in osteogenic medium and 4 h miR-29b transfection; 4] miR-29b + Dox: cultured in osteogenic medium plus 1.8 µM of Doxorubicin and 4 h miR-29b transfection.

After 1 week, tumor spheroids were liberated from the microwells as previously described.[7] Spheroids were prepared in one of the following ways: 1) snap-frozen and stored at −80 °C for DNA analysis; 2) harvested and aliquoted for flow cytometry; 3) snap-frozen using liquid nitrogen and stored at −80 °C for PCR analysis, or 4) embedded within 2% agarose and fixed overnight in 4% paraformaldehyde before being placed in PBS and refrigerated for histochemical analysis.

DNA Analysis: To assess DNA content for all constructs, 0.5 mL of papain digestion buffer (100 mm sodium phosphate buffer containing 10 mm L-cysteine [Sigma-Aldrich], 125 µg mL^{-1} papain [Sigma-Aldrich], and 5 mM Na2EDTA [Sigma-Aldrich] in ddH2O at pH 6.5) was added to the spheroids that were placed on a rotator in an oven at 60 °C overnight, as previously described.[7] Once the spheroids were digested, DNA content was performed using Quant-iT PicoGreen dsDNA Assay.

Calcium Deposition: Calcium deposition within the tumor spheroids was measured using the Calcium LiquiColor Test (Stanbio Laboratories) according to the manufacturer's protocol. Briefly, a cell lysate was prepared by digesting the spheroids in a 0.5 M hydrochloric acid solution at 60 °C overnight, as previously described.[7,57]

PCR Analysis: RNA from spheroids (MSCs spheroids, SaOS2 spheroids, or co-culture spheroids) was extracted using Trizol Reagent and assessed for concentration and purity using the NanoDrop 2000c UV–vis spectrophotometer. RNA was equalized and reverse transcribed using the Applied Biosystems High-Capacity cDNA reverse transcription kit. Real-time PCR was carried out on triplicate cDNA samples with the use of the CFX96 Touch Real-Time PCR Detection System (Bio-Rad Laboratories, California). Real-time PCR for the detection of *MMP2, MMP9, β-Catenin, BCL-2, Caspase 9, Caspase 3*, and *BAX* mRNA was performed using the TaqMan fast universal PCR Master Mix (Applied Biosystems) and predesigned TaqMan gene expression primers. mRNA amounts were normalized relative to the housekeeping gene Ribosomal Protein 18s. For the assessment of growth factor gene expression Sigma primers for *VEGF, RUNX2, Col1A, TGFβ3*, and *ALP* (Table S1, Supporting Information) were used, and mRNA amounts were normalized to glyceraldehyde 3-phosphate dehydrogenase (GAPDH) as housekeeping gene.

Flow Cytometry—Cell Tracking: Prior to cell seeding MSCs and SaOS2 cells were stained with cell tracker dyes; QTracker705 and QTracker585 (Thermo Fisher), respectively, as previously described.[7] Cells were seeded and transfected and cultured for a further 7 further days under their respective culture conditions. Following 1 week of cultures, spheroids were harvested and aliquoted into triplicates such that there was a minimum of 100 spheroids per sample. A single-cell suspension was created by incubating the tumor spheroids with 0.25% Trypsin-EDTA at 37 °C for 15 min. Following 1 wash with PBS, cells were stained with LIVE/DEAD Fixable Near–IR fluorescent dye (L10119,

Thermo Fisher) according to the manufacturer's instructions. Following fixation, the cell suspensions were analyzed by flow cytometry using a BD LSR II HTS-1 flow cytometer (BD Biosciences) to determine the ratio of MSC+ to SaOS2+ cells for each culture condition. All data were analyzed using Flowjo software (Flowjo LLC), gating strategy could be found in Figure S7 (Supporting Information).

Histology: Following embedding within 2% agarose and fixation, overnight samples were dehydrated and embedded in paraffin using an automatic tissue processor (ASP300; Leica, London, UK). All samples were sectioned at a thickness of 6 µm using a rotary microtome (Leica). Sections were stained with H&E and 2% Alizarin Red solution (all Sigma-Aldrich).

Preparation of Transfected Wild-Type K7M2 Cells: K7M2 WT cells were seeded into a 96-Well White/Clear Bottom Plate (Thermo Fisher, 165306) at a seeding density of 2×10^4 cells in 100 µL per well. To determine the

optimum transfection ratio multiple complexes were created (1.5:1, 3:1, 6:1) using ViaFect Transfection reagent (Promega, E4981) and pGL4.51 [luc2/CMV/Neo] plasmid vector (Promega, E1320) as per the manufacturer's specifications and incubated with K7M2 cells for 24 h. Following 24 h of incubation the cells were washed twice with PBS and fresh medium was added to the cells after which they were further cultured for another 48 h. The selective drug Geneticin-418 (Thermo Fisher, 10131035) was then added at a concentration of 200 μg mL^{-1} to kill non-transfected cells. To validate transfection and determine optimum transfection ratio in vitro bioluminescence imaging was performed. Briefly, a 200× Luciferin stock solution (30 mg mL^{-1}) was prepared in sterile water. From that stock solution, a 150 μg mL^{-1} working solution was prepared in an expansion medium. The working solution was added directly onto the transfected K7M2 cells and bioluminescence was measured using Infinite M Plex (Tecan) plate reader every 10 min, up to 40 min to determine the kinetic curve and find the peak imaging timepoint for the cells (Figure S8A, Supporting Information).

For in vivo inoculation transfected K7M2 osteosarcoma cells were prepared by seeding 6×10^5 cells into each well of a six-well plate. A 6:1 transfection ratio complex was created as was deemed the optimum transfection ratio and the K7M2 cells transfected with the luciferase reporter as described above.

To assess the stability of the luciferase reporter in vitro bioluminescence imaging was performed on the transfected K7M2 cells for multiple cell passages (Figure S8B, Supporting Information). Passage two transfected cells were used for orthotopic implantation.

Development of Metastatic Osteosarcoma Murine Model: All mouse procedures were conducted at the Koch Institute for Integrative Cancer Research at the Massachusetts Institute of Technology (MIT) under the protocol approved for this study by the Institutional Animal Care and Use Committee (IACUC). To assess the optimum concentration of osteosarcoma cells needed to induce tumor formation, two concentrations of transfected K7M2 cells were evaluated 0.3×10^6 cells and 1×10^6 cells.[27] Six female BALB/c mice (3 0.3×10^6 cells, 3 1×10^6 cells) aged 6 weeks underwent inoculation with either of the cell concentrations (Figure S9, Supporting Information). Briefly, the BALB/c mice were anesthetized using 2% isoflurane. Analgesia, slow-release buprenorphine (1 mg kg^{-1}) was administered subcutaneously. A small incision into the skin above the tibial plateau was made and the muscle was dissected away. A small hole was created on the tibial plateau into the medullary canal using a 26G needle. 10 μL of the luciferase labeled K7M2 cells at either concentration was injected into the proximal tibia using a 27G Hamilton syringe.

Synthesis of Amino-Modified Hyaluronic Acid (HA-SS-NH2): Synthesis of HA-SS- NH_2 was performed as previously described.[59] Briefly, 60 kDa-sodium hyaluronate (1% w/v in MES buffer) was modified with cysteamine dihydrochloride through *N*-(3-(dimethylamino)propyl)carbodiimide (EDC) and *N*-hydroxysuccinimide (NHS) chemistry. The reaction was performed at room temperature for 12 h. The product HA-SS-NH2 was purified by dialysis, freeze-dried, and stored at −20 °C. HA-SS-NH2 polymer structure was confirmed by 1H-NMR (400 MHz Varian (NMR Instruments, Clarendon Hills, IL, USA)).

Development of a Hyaluronic Acid (HA) Injectable Delivery System: Amine-modified hyaluronic acid was dissolved in phosphate buffer (pH = 7.4) containing the miR-29b-pBAE nanoparticles to obtain a 10% (w/v) HA solution. 8-arm-PEG-NHS crosslinker was also dissolved in phosphate buffer (pH = 7.4) to obtain a 10% (w/v) solution. For in vitro, the two polymer solutions were vigorously mixed together for 10 s inside cylindrical plastic molds (diameter: 5.00 mm; height: 2.50 mm). Hydrogel disks were allowed to react for 5 min to ensure full gelation. For in vivo, the two polymer solutions were loaded in a double-channel syringe coupled to a mixer allowing the hydrogel formation once injected.

Characterization of HA Injectable Delivery System: To measure the swelling ratio of the hydrogel, the two polymer solutions were vigorously mixed together for 10 s inside cylindrical plastic molds (diameter: 5.00 mm; height: 2.50 mm). Hydrogel disks were weighed and then placed in 1 ml of PBS. At each time point (15 min, 30 min, 1, 2, 4, 8, and 24 h) the disks were weighed before being placed back into the PBS.

To measure the gelation kinetics of the hydrogel, hydrogel disks were formed on cylindrical molds as described above and timed from initial mixing, the start of the gelation, and finally until the disks were fully formed and cross-linked. The cross-linking was deemed finished when the hydrogel disks could be easily removed from the mold.

To measure the compressive modulus of the hydrogel, hydrogel disks were formed on cylindrical molds as described above. Disks were placed in the Universal Testing Machine (Instron, 6800 Series Universal Testing) and a compression test was performed following the protocol from the manufacturer, with a ramp of 2 N up to 100 N. The compression test was analyzed with Bluehill Universal (v4.13, Instron) and origin (v9.8, OriginLab). Compressive modulus was calculated with the slope within the linear section of the strain–stress curve, ranging between 5–15%.

Cellular Uptake and Biological Activity of miR-29b after Release of Nanoparticles from HA Injectable Delivery System: To ensure that the miR-29b is still functional following loading within the HA injectable delivery system the cellular uptake and biological activity of miR-29b were assessed. Briefly, the HA delivery system loaded with either pBAE:miR-29b (Hydrogel + miR-29b NPs) complexes or PBS (Hydrogel alone) was prepared. The hydrogels were injected into cylindrical plastic molds (diameter: 5.00 mm; height: 2.50 mm) to create hydrogel disks and were cultured in PBS for 6 days in normoxic conditions. During this time the conditioned medium was collected and after 6 days of release analyzed the medium for fluorescence using a standard curve to calculate the concentration of nanoparticles within the medium. SaOS2 cells and human MSCs were seeded at 2×10^4 cells cm^{-2} in a standard 24-well plate. After seeding, cells were transfected for 4 h with the release of the hydrogels with 20 nM of pBAE:miR-29b complexes or the equivalent of empty hydrogels and 20 nM of fresh pBAE:miR-29b (miR-29b NPs alone) complexes as a positive control. ALP expression and DNA content were assessed in MSCs after a further 7 days of culture and in SaOS2 cells after a further 3 days of culture as described above.

Surgical Procedure: Forty female BALB/c mice aged 6 weeks underwent inoculation with 0.3×10^6 K7M2-Luc cells according to the same protocol as mentioned above. The average mouse weight was 18.5 g at the time of inoculation. Palpable tumors were allowed to form for two weeks and once a suitable-sized tumor has formed, the animals ($n = 8$) were randomly assigned into different treatment groups: 1] No Treatment: Tumor cell inoculation with no further treatment; 2] Dox Alone: Tumor cell inoculation plus tail vein (i.v.) injection of Doxorubicin (Fisher, BP2516-10) 2 mg kg^{-1} biweekly for three weeks; 3] Hydrogel Alone: mice were anesthetized with 1–2% isoflurane and non-invasively 100 μL of HA hydrogel were injected around the tumor site; 4] miR-29b: mice were anesthetized with 1–2% isoflurane and non-invasively 100 μL of HA hydrogel loaded with fluorescently-labeled (640 ex, 680 em) pBAE:miR-29b nanoparticles (750 μg kg^{-1} miR-29b) was injected around the tumor site. This concentration of miR-29b had previously been shown to significantly reduce tumor growth in non-small-cell lung cancer;[60] 5] miR-29b + Dox: mice were anesthetized with 1–2% isoflurane and non-invasively 100 μL of HA hydrogel loaded with fluorescently-labeled pBAE:miR-29b nanoparticles were injected around the tumor site. Following hydrogel implantation mice were treated with i.v. injection of Doxorubicin (2 mg kg^{-1}) biweekly for three weeks. Thirty-one out of forty mice grew primary tumors.

The tumor size was measured twice a week via caliper measurements, and the tumor volume was calculated using the following formulas: leg volume = length × $(\text{width})^2 \times 0.5$; tumor volume = leg Volume on day X/leg Volume on day 0. Body weight was measured contemporaneously with tumor volume. Mice were euthanized when tumors reached a volume of 1000 mm^3 or for otherwise poor body conditions. Nine mice were removed from the study as no bioluminescent signal was recorded and no palpable tumor formed in these mice in the 45 days following tumor cell inoculation.

Bioluminescence (BLI) Imaging: Briefly, mice were shaved and then anesthetized with 1–2% isoflurane using a calibrated vaporizer inside an IVIS Spectrum (PerkinElmer). Non-invasive longitudinal monitoring of tumor progression and nanoparticle release was followed by

scanning mice with the IVIS Spectrum-bioluminescent and fluorescent imaging system (PerkinElmer). Luciferin (150 mg kg^{-1}) was injected intraperitoneally and at each time point, a kinetic curve was performed to determine the peak signal time (≈15–20 min). Whole-animal bioluminescent and fluorescent imaging was performed biweekly for 18 days following treatment.

X-ray Microtomography (μCT): Micro-CT images of the tibias were performed in Skyscan 1276 (Bruker) μCT pre-treatment, 2- and 4-weeks post-treatment to monitor osteolysis and metastasis. Briefly, mice were anesthetized with 1–2% isoflurane using a calibrated vaporizer inside a Skyscan 1276 μCT and noninvasively imaged. Scans were performed using a voxel resolution of 16 μm. Data were analyzed using ImageJ BoneJ plugin.

Histological Analysis: All of the tibias were removed from the mice at their respective endpoints and fixed overnight at 4 °C in 10% formalin. Tibias were also decalcified for 1 week before tissue processing. All samples were dehydrated and embedded in paraffin using an automatic tissue processor (Leica ASP300, Leica). All samples were sectioned with a thickness of 8 μm using a rotary microtome (Leica Microtome RM2235, Leica). Sections were stained with H&E to assess tumor growth or Goldner's Trichrome to assess bone regeneration.

BMP-2 Delivery: To validate the clinical relevance of localized delivery of miR-29b to induce bone remodeling within the bone and normalized the dysregulation of bone homeostasis caused by the tumor and chemotherapeutics, the bone formation potential was directly compared to BMP-2 delivery which was known to induce bone formation. Sixteen BALB/c mice aged 6 weeks underwent inoculation with 0.3×10^6 K7M2 cells according to the same protocol as mentioned above. Once a suitable-sized tumor had formed, the animals ($n = 8$) were randomly assigned into two different treatment groups: 1] BMP-2: mice were anesthetized with 1–2% isoflurane and non-invasively 100 μL of HA hydrogel loaded with 5 μg BMP-2[34] (Peprotech, 120-02) were injected around the tumor site; 2] BMP-2 + Dox: mice were anesthetized with 1–2% isoflurane and non-invasively 100 μL of HA hydrogel loaded with were injected around the tumor site. Following hydrogel implantation mice were treated with i.v. injection of Doxorubicin (2 mg kg^{-1}) biweekly for three weeks. Tumor volume and body weight were measured every other day. Six mice were removed from the study as no bioluminescent signal was recorded and no palpable tumor formed in these mice in the 45 days following tumor cell inoculation.

BMP-2 Enzyme-Linked Immunosorbent Assay (ELISA): For in vitro BMP-2 release studies, the two polymer solutions (loaded with 5 μg BMP-2) were vigorously mixed together for 10 s inside cylindrical plastic molds (diameter: 5.00 mm; height: 2.50 mm). Hydrogel disks were allowed to react for 5 min to ensure full gelation. The hydrogels were then cultured in expansion media for 35 days in culture. A BMP-2 ELISA (R&D systems) was used to quantify the levels of BMP-2 released by the hydrogels. The cell culture media were analyzed at the specific time points detailed above. Assays were carried out per the manufacturer's protocol and analyzed on a microplate reader at a wavelength of 450 nм.

Statistical Analysis: Results were expressed as mean ± standard deviation. Statistical analysis was performed using the following variables: 1) when there were two groups and one time-point a standard two-tailed t-test was performed; 2) when there were more than two groups and one time-point a one-way analysis of variance (ANOVA) was performed; and 3) when there were more than two groups and multiple time points a two-way ANOVA was performed. For in vivo studies, multiple comparisons among groups were determined using Kruskal–Wallis test with uncorrected Dunn's test. Kaplan–Meier survival curve statistical analysis was determined using the two-tailed Mantel–Cox test. No specific preprocessing of data was performed prior to statistical analysis. All analyzes were performed using GraphPad (GraphPad Software, La Jolla California USA, http://www.graphpad.com). For all comparisons, the level of significance was $p \leq 0.05$.

Supporting Information

Supporting Information is available from the Wiley Online Library or from the author.

Acknowledgements

This project has received funding from the European Union's Horizon 2020 Research and Innovation Program under the Marie Skłodowska-Curie Grant Agreement No. 839150 and the Gillian Reny Stepping Strong Center for Trauma Innovation. The authors thank the Division of Comparative Medicine at MIT for the assistance with animal housing. The authors thank Swanson Biotechnology Center at the Koch Institute for Integrative Cancer Research at the Massachusetts Institute of Technology (MIT) for assistance with animal experiments and facilities, especially the microscopy, preclinical imaging and testing, flow cytometry, and histology cores. The authors thank Dr. A.M. Hayward for clinical assistance in developing the osteosarcoma murine model. The authors thank G. Paradis for FACS assistance with Cancer Center Support (FACS core). The authors thank Kathleen S. Cormier for her histology assistance. The authors thank M. Cornwall-Brady for assistance with μCT scanning and analysis. The authors thank J. Kuhn for confocal imaging assistance. Research undertaken in Daniel Kelly's laboratory at Trinity College Dublin is part-funded by Johnson & Johnson.

Conflict of Interest

The authors declare no conflict of interest.

Author Contributions

F.E.F was responsible for technical design, development of osteosarcoma tumor model, all in vitro pre-screening experiments, developing the osteosarcoma animal model, performing all of the animal surgeries, all IVIS imaging and CT scans, data interpretation, histological analysis and drafting the paper. P.D.P. assisted with animal surgeries and developed and characterized the pBAE nanoparticles and HA injectable delivery system. C.R.R.J and N.R.T assisted with the characterization and in vitro release profile of the pBAE nanoparticles from the HA hydrogel. O.M. helped with all of the PCR analysis. L.C.S assisted with the Annexin V/PI co-staining procedure and the immunoblotting. D.J.K. and N.A. conceived and helped design the experiments, oversaw the collection of results and data interpretation and finalized the paper.

Data Availability Statement

The data that support the findings of this study are available from the corresponding author upon reasonable request.

Keywords

biomaterials, bone regenerations, microRNAs, nanoparticles, osteosarcoma

Received: August 29, 2022
Revised: March 6, 2023
Published online: April 25, 2023

[1] A. Misaghi, A. Goldin, M. Awad, A. A. Kulidjian, *SICOT J.* **2018**, *4*, 12.
[2] *The Ortho Factbook*, 2nd ed. Knowledge Enterprises Inc, Chagrin Falls, OH, USA **2001**.
[3] a) T. M. Fan, R. D. Roberts, M. M. Lizardo, *Front. Oncol.* **2020**, *10*, 13; b) K. Winkler, G. Beron, G. Delling, U. Heise, H. Kabisch, C. Purfürst, J. Berger, J. Ritter, H. Jürgens, V. Gerein, *J. Clin. Oncol.* **1988**, *6*, 329; c) N. M. Marina, S. Smeland, S. S. Bielack, M. Bernstein, G. Jovic,

M. D. Krailo, J. M. Hook, C. Arndt, H. van den Berg, B. Brennan, B. Brichard, K. L. B. Brown, T. Butterfass-Bahloul, G. Calaminus, H. E. Daldrup-Link, M. Eriksson, M. C. Gebhardt, H. Gelderblom, J. Gerss, R. Goldsby, A. Goorin, R. Gorlick, H. E. Grier, J. P. Hale, K. S. Hall, J. Hardes, D. S. Hawkins, K. Helmke, P. C. W. Hogendoorn, M. S. Isakoff, *Lancet Oncol.* **2016**, *17*, 1396; d) S. S. Bielack, S. Smeland, J. S. Whelan, N. Marina, G. Jovic, J. M. Hook, M. D. Krailo, M. Gebhardt, Z. Pápai, J. Meyer, H. Nadel, R. L. Randall, C. Deffenbaugh, R. Nagarajan, B. Brennan, G. D. Letson, L. A. Teot, A. Goorin, D. Baumhoer, L. Kager, M. Werner, C. C. Lau, K. Sundby Hall, H. Gelderblom, P. Meyers, R. Gorlick, R. Windhager, K. Helmke, M. Eriksson, P. M. Hoogerbrugge, *J. Clin. Oncol.* **2015**, *33*, 2279.

[4] a) A. Luetke, P. A. Meyers, I. Lewis, H. Juergens, *Cancer Treat. Rev.* **2014**, *40*, 523; b) H. T. Ta, C. R. Dass, I. Larson, P. F. Choong, D. E. Dunstan, *Biomaterials* **2009**, *30*, 3605.

[5] N. Omer, M. C. Le Deley, S. Piperno-Neumann, P. Marec-Berard, A. Italiano, N. Corradini, C. Bellera, L. Brugières, N. Gaspar, *Eur. J. Cancer* **2017**, *75*, 98.

[6] a) A. Lamora, J. Talbot, M. Mullard, B. Brounais-Le Royer, F. Redini, F. Verrecchia, *J. Clinic. Med.* **2016**, *5*, 96; b) Z. Yao, B. Murali, Q. Ren, X. Luo, D. V. Faget, T. Cole, B. Ricci, D. Thotala, J. Monahan, J. M. van Deursen, D. Baker, R. Faccio, J. K. Schwarz, S. A. Stewart, *Cancer Res.* **2020**, *80*, 1171; c) O. K. Lee, M. J. Coathup, A. E. Goodship, G. W. Blunn, *Tissue Eng.* **2005**, *11*, 1727; d) K. C. Stine, E. C. Wahl, L. Liu, R. A. Skinner, J. Vanderschilden, R. C. Bunn, C. O. Montgomery, L. J. Suva, J. Aronson, D. L. Becton, R. W. Nicholas, C. J. Swearingen, C. K. Lumpkin Jr, *J. Orthop. Res.* **2014**, *32*, 464; e) A. Alfranca, L. Martinez-Cruzado, J. Tornin, A. Abarrategi, T. Amaral, E. de Alava, P. Menendez, J. Garcia-Castro, R. Rodriguez, *Cell. Mol. Life Sci.* **2015**, *72*, 3097.

[7] F. E. Freeman, R. Burdis, O. R. Mahon, D. J. Kelly, N. Artzi, *Adv. Healthcare Mater.* **2022**, *11*, 2101296.

[8] a) Y. Deng, H. Zhou, P. Gu, X. Fan, *Invest Ophthalmol Vis Sci* **2014**, *55*, 6016; b) A. Gilam, J. Conde, D. Weissglas-Volkov, N. Oliva, E. Friedman, N. Artzi, N. Shomron, *Nat. Commun.* **2016**, *7*, 12868.

[9] B. Yan, Q. Guo, F. J. Fu, Z. Wang, Z. Yin, Y. B. Wei, J. R. Yang, *OncoTargets Ther.* **2015**, *8*, 539.

[10] a) M. J. Schmitt, C. Margue, I. Behrmann, S. Kreis, *Curr. Mol. Med.* **2013**, *13*, 572; b) S. Sur, R. Steele, X. Shi, R. B. Ray, *Cells* **2019**, *8*; c) L. H. Wang, J. Huang, C. R. Wu, L. Y. Huang, J. Cui, Z. Z. Xing, C. Y. Zhao, *Mol. Med. Rep.* **2018**, *17*, 2113; d) G. Song, Y. Zhou, R. Chen, Q. Li, B. Shan, Y. Duan, Y. Wang, *Clin. Lab.* **2016**, *62*, 1739; e) Y. Teng, Y. Zhang, K. Qu, X. Yang, J. Fu, W. Chen, X. Li, *OncoTargets Ther.* **2015**, *6*, 40799.

[11] J. Shin, H. G. Shim, T. Hwang, H. Kim, S.-H. Kang, Y.-S. Dho, S.-H. Park, S. J. Kim, C.-K. Park, *Cancer Cell Int.* **2017**, *17*, 104.

[12] a) Z. Li, M. Q. Hassan, M. Jafferji, R. I. Aqeilan, R. Garzon, C. M. Croce, A. J. van Wijnen, J. L. Stein, G. S. Stein, J. B. Lian, *J. Biol. Chem.* **2009**, *284*, 15676; b) M. Rossi, M. R. Pitari, N. Amodio, M. T. Di Martino, F. Conforti, E. Leone, C. Botta, F. M. Paolino, T. Del Giudice, E. Iuliano, M. Caraglia, M. Ferrarini, A. Giordano, P. Tagliaferri, P. Tassone, *J. Cell. Physiol.* **2013**, *228*, 1506.

[13] a) H. X. Chen, X. X. Xu, B. Z. Tan, Z. Zhang, X. D. Zhou, *Cell. Physiol. Biochem.* **2017**, *41*, 933; b) J. H. Fang, H. C. Zhou, C. Zeng, J. Yang, Y. Liu, X. Huang, J. P. Zhang, X. Y. Guan, S. M. Zhuang, *Hepatology* **2011**, *54*, 1729; c) Y. Li, B. Cai, L. Shen, Y. Dong, Q. Lu, S. Sun, S. Liu, S. Ma, P. X. Ma, J. Chen, *Cancer Lett* **2017**, *397*, 111; d) S. Sur, R. Steele, X. Shi, R. B. Ray, *Cells* **2019**, *8*, 1455.

[14] a) K. Zhu, L. Liu, J. Zhang, Y. Wang, H. Liang, G. Fan, Z. Jiang, C. Y. Zhang, X. Chen, G. Zhou, *Protein Cell* **2016**, *7*, 434; b) W. Xu, Z. Li, X. Zhu, R. Xu, Y. Xu, *Med Sci Monit* **2018**, *24*, 8812; c) K. Zhang, C. Zhang, L. Liu, J. Zhou, *Int. J. Clin. Exp. Pathol.* **2014**, *7*, 5701.

[15] D. J. Luo, L. J. Li, H. F. Huo, X. Q. Liu, H. W. Cui, D. M. Jiang, *Riv. Eur. Sci. Med. Farmacol.* **2019**, *23*, 1434.

[16] Y. Chen, D. Y. Gao, L. Huang, *Adv. Drug Delivery Rev.* **2015**, *81*, 128.

[17] a) M. Guvendiren, H. D. Lu, J. A. Burdick, *Soft Matter* **2012**, *8*, 260; b) L. L. Wang, Y. Liu, J. J. Chung, T. Wang, A. C. Gaffey, M. Lu, C. A. Cavanaugh, S. Zhou, R. Kanade, P. Atluri, E. E. Morrisey, J. A. Burdick, *Nat. Biomed. Eng.* **2017**, *1*, 983.

[18] E. Larrañeta, M. Henry, N. J. Irwin, J. Trotter, A. A. Perminova, R. F. Donnelly, *Carbohydr. Polym.* **2018**, *181*, 1194.

[19] N. Puigmal, P. Dosta, Z. Solhjou, K. Yatim, C. Ramírez, J. Y. Choi, J. B. Alhaddad, A. P. Cosme, J. Azzi, N. Artzi, *Adv. Funct. Mater.* **2021**, *31*, 2100128.

[20] P. Dosta, I. Tamargo, V. Ramos, S. Kumar, D. W. Kang, S. Borrós, H. Jo, *Adv. Healthcare Mater.* **2021**, *10*, 2001894.

[21] a) J. C. Sunshine, S. B. Sunshine, I. Bhutto, J. T. Handa, J. J. Green, *PLoS One* **2012**, *7*, e37543; b) X. Gao, Z. Jin, X. Tan, C. Zhang, C. Zou, W. Zhang, J. Ding, B. C. Das, K. Severinov, I. I. Hitzeroth, *J. Controlled Release* **2020**, *321*, 654; c) D. M. Lynn, R. Langer, *J. Am. Chem. Soc.* **2000**, *122*, 10761.

[22] T. Zhang, X. Xue, H. Peng, *Mol. Ther.* **2019**, *27*, 1183.

[23] A. Mikai, M. Ono, I. Tosa, H. T. T. Nguyen, E. S. Hara, S. Nosho, A. Kimura-Ono, K. Nawachi, T. Takarada, T. Kuboki, T. Oohashi, *Int. J. Mol. Sci.* **2020**, *21*, 7028.

[24] P. Dosta, V. Ramos, S. Borrós, *Mol. Syst. Des. Eng.* **2018**, *3*, 677.

[25] P. Dosta, C. Demos, V. Ramos, D. W. Kang, S. Kumar, H. Jo, S. Borrós, *Cardiovasc. Eng. Technol.* **2021**, *12*, 114.

[26] N. Segovia, P. Dosta, A. Cascante, V. Ramos, S. Borrós, *Acta Biomater.* **2014**, *10*, 2147.

[27] B. T. Grisez, J. J. Ray, P. A. Bostian, J. E. Markel, B. A. Lindsey, *J. Orthop. Res.* **2018**, *36*, 2294.

[28] a) E. Christidi, L. R. Brunham, *Cell Death Dis.* **2021**, *12*, 339; b) A.-M. Meredith, C. R. Dass, *J. Pharm. Pharmacol.* **2016**, *68*, 729.

[29] M. Cortini, N. Baldini, S. Avnet, *Front. Physiol.* **2019**, *10*, 814.

[30] a) J. Han, B. Yong, C. Luo, P. Tan, T. Peng, J. Shen, *World J. Surg. Oncol.* **2012**, *10*, 37; b) J. Zhou, T. Liu, W. Wang, *Medicine* **2018**, *97*, 13051; c) P. Kunz, H. Sähr, B. Lehner, C. Fischer, E. Seebach, J. Fellenberg, *BMC Cancer* **2016**, *16*, 223; d) J. Wang, Q. Shi, T.-x. Yuan, Q.-l. Song, Y. Zhang, Q. Wei, L. Zhou, J. Luo, G. Zuo, M. Tang, T.-C. He, Y. Weng, *Clin. Chim. Acta* **2014**, *433*, 225.

[31] N. Segovia, M. Pont, N. Oliva, V. Ramos, S. Borrós, N. Artzi, *Adv. Healthcare Mater.* **2015**, *4*, 271.

[32] a) G. Hulsart-Billström, K. Bergman, B. Andersson, J. Hilborn, S. Larsson, K. B. Jonsson, *J. Tissue Eng. Regener. Med.* **2015**, *9*, 799; b) S. W. Jung, J. H. Byun, S. H. Oh, T. H. Kim, J. S. Park, G. J. Rho, J. H. Lee, *Carbohydr. Polym.* **2018**, *180*, 216; c) C. Martínez-Álvarez, B. González-Meli, B. Berenguer-Froehner, I. Paradas-Lara, Y. López-Gordillo, C. Rodríguez-Bobada, P. González, M. Chamorro, P. Arias, J. Hilborn, I. Casado-Gómez, E. Martínez-Sanz, *J. Surg. Res.* **2013**, *183*, 654; d) E. Martínez-Sanz, D. A. Ossipov, J. Hilborn, S. Larsson, K. B. Jonsson, O. P. Varghese, *J. Controlled Release* **2011**, *152*, 232; e) E. Martínez-Sanz, O. P. Varghese, M. Kisiel, T. Engstrand, K. M. Reich, M. Bohner, K. B. Jonsson, T. Kohler, R. Müller, D. A. Ossipov, J. Hilborn, *J. Tissue Eng. Regener. Med.* **2012**, *6*, s15; f) S. H. Park, J. Y. Park, Y. B. Ji, H. J. Ju, B. H. Min, M. S. Kim, *Acta Biomater.* **2020**, *117*, 108.

[33] P. D. Ottewell, J. K. Woodward, D. V. Lefley, C. A. Evans, R. E. Coleman, I. Holen, *Mol. Cancer Ther.* **2009**, *8*, 2821.

[34] a) F. E. Freeman, P. Pitacco, L. H. A. van Dommelen, J. Nulty, D. C. Browe, J. Y. Shin, E. Alsberg, D. J. Kelly, *Sci. Adv.* **2020**, *6*, eabb5093; b) Y. M. Kolambkar, K. M. Dupont, J. D. Boerckel, N. Huebsch, D. J. Mooney, D. W. Hutmacher, R. E. Guldberg, *Biomaterials* **2011**, *32*, 65; c) J. D. Boerckel, Y. M. Kolambkar, K. M. Dupont, B. A. Uhrig, E. A. Phelps, H. Y. Stevens, A. J. García, R. E. Guldberg, *Biomaterials* **2011**, *32*, 5241; d) M. Kisiel, M. M. Martino, M. Ventura, J. A. Hubbell, J. Hilborn, D. A. Ossipov, *Biomaterials* **2013**, *34*, 704.

[35] A. Forterre, H. Komuro, S. Aminova, M. Harada, *Cancers (Basel)* **2020**, *1*, 1852.

[36] a) F. Barzegari Firouzabadi, S. H. Oryan, M. H. Sheikhha, S. M. Kalantar, A. Javed, *Cell J.* **2019**, *21*, 135; b) D. F. Chen, B. W. Zhang, J. Cao, H. Wang, P. Luo, W. Liu, X. Niu, R. Wang, J. J. Nie, *Biomater. Sci.* **2022**, *10*, 2844; c) M. Gong, H. Liu, N. Sun, Y. Xie, F. Yan, L. Cai, *Nanomedicine* **2020**, *15*, 711; d) H. He, J. Ni, J. Huang, *Oncol. Lett.* **2014**, *7*, 1352; e) T. Luo, X. Zhou, E. Jiang, L. Wang, Y. Ji, Z. Shang, *Front. Oncol.* **2021**, *11*, 618662; f) L. Ou, H. Lin, Y. Song, G. Tan, X. Gui, J. Li, X. Chen, Z. Deng, S. Lin, *Int. J. Nanomed.* **2020**, *15*, 5131; g) D. D. Rao, C. Jay, Z. Wang, X. Luo, P. Kumar, H. Eysenbach, M. Ghisoli, N. Senzer, J. Nemunaitis, *Mol. Ther.* **2016**, *24*, 1412; h) K. Shimbo, S. Miyaki, H. Ishitobi, Y. Kato, T. Kubo, S. Shimose, M. Ochi, *Biochem. Biophys. Res. Commun.* **2014**, *445*, 381; i) K. Zhang, C. Dong, M. Chen, T. Yang, X. Wang, Y. Gao, L. Wang, Y. Wen, G. Chen, X. Wang, X. Yu, Y. Zhang, P. Wang, M. Shang, K. Han, Y. Zhou, *Theranostics* **2020**, *10*, 411; j) L. Zhang, A. K. Lyer, X. Yang, E. Kobayashi, Y. Guo, H. Mankin, F. J. Hornicek, M. M. Amiji, Z. Duan, *Int. J. Nanomed.* **2015**, *10*, 2913.

[37] A. Gupta, R. Bahal, M. Gupta, P. M. Glazer, W. M. Saltzman, *J. Controlled Release* **2016**, *240*, 302.

[38] A. Tchoryk, V. Taresco, R. H. Argent, M. Ashford, P. R. Gellert, S. Stolnik, A. Grabowska, M. C. Garnett, *Bioconjugate Chem.* **2019**, *30*, 1371.

[39] a) M. Vinci, S. Gowan, F. Boxall, L. Patterson, M. Zimmermann, W. Court, C. Lomas, M. Mendiola, D. Hardisson, S. A. Eccles, *BMC Biol.* **2012**, *10*, 29; b) A. Ivascu, M. Kubbies, *J. Biomol. Screening* **2006**, *11*, 922; c) A. S. Mikhail, S. Eetezadi, C. Allen, *PLoS One* **2013**, *8*, 62630.

[40] a) A. Pluen, Y. Boucher, S. Ramanujan, T. D. McKee, T. Gohongi, E. d. Tomaso, E. B. Brown, Y. Izumi, R. B. Campbell, D. A. Berk, R. K. Jain, *Proc. Natl. Acad. Sci. USA* **2001**, *98*, 4628; b) H. Cabral, Y. Matsumoto, K. Mizuno, Q. Chen, M. Murakami, M. Kimura, Y. Terada, M. R. Kano, K. Miyazono, M. Uesaka, N. Nishiyama, K. Kataoka, *Nat. Nanotechnol.* **2011**, *6*, 815.

[41] H.-X. Wang, Z.-Q. Zuo, J.-Z. Du, Y.-C. Wang, R. Sun, Z.-T. Cao, X.-D. Ye, J.-L. Wang, K. W. Leong, J. Wang, *Nano Today* **2016**, *11*, 133.

[42] a) K. B. Jones, Z. Salah, S. Del Mare, M. Galasso, E. Gaudio, G. J. Nuovo, F. Lovat, K. LeBlanc, J. Palatini, R. L. Randall, S. Volinia, G. S. Stein, C. M. Croce, J. B. Lian, R. I. Aqeilan, *Cancer Res.* **2012**, *72*, 1865; b) N. Dai, Z. Y. Zhong, Y. P. Cun, Y. Qing, C. Chen, P. Jiang, M. X. Li, D. Wang, *Neoplasma* **2013**, *60*, 384.

[43] a) C. L. Klatt, V. Theis, S. Hahn, C. Theiss, V. Matschke, *Cells* **2019**, *8*, 1077; b) Z. Qin, X. Wang, Y. Zhou, J. Zheng, H. Li, L. Li, *Apoptosis* **2023**, *28*, 210; c) O. Sul, H.-S. Choi, *FASEB J.* **2019**, *33*, 77816; d) O.-J. Sul, M. Rajasekaran, H.-J. Park, J.-H. Suh, H.-S. Choi, *Oxid. Med. Cell. Longevity* **2019**, *2019*, 6018180.

[44] T. Xia, S. Dong, J. Tian, *Int. J. Mol. Med.* **2020**, *46*, 709.

[45] a) T. Nakasa, M. Yoshizuka, M. Andry Usman, E. Elbadry Mahmoud, M. Ochi, *Curr. Genomics* **2015**, *16*, 441; b) K. Kapinas, C. Kessler, T. Ricks, G. Gronowicz, A. M. Delany, *J. Biol. Chem.* **2010**, *285*, 25221; c) Q. Zeng, Y. Wang, J. Gao, Z. Yan, Z. Li, X. Zou, Y. Li, J. Wang, Y. Guo, *Cell. Mol. Biol. Lett.* **2019**, *24*, 11; d) T. Xia, S. Dong, J. Tian, *Int. J. Mol. Med.* **2020**, *46*, 709.

[46] a) B. Cai, L. Huang, J. Wang, D. Sun, C. Zhu, Y. Huang, S. Li, Z. Guo, L. Liu, G. Feng, Y. Li, L. Zhang, *Bioconjugate Chem.* **2021**, *32*, 2184; b) W. Diwu, X. Dong, O. Nasif, S. A. Alharbi, J. Zhao, W. Li, *Front. Cell Dev. Biol.* **2020**, *8*, 631107; c) S. Dong, Y. N. Zhang, J. Wan, R. Cui, X. Yu, G. Zhao, K. Lin, *J. Mater. Chem. B* **2020**, *8*, 368; d) C. He, C. Dong, L. Yu, Y. Chen, Y. Hao, *Adv. Sci.* **2021**, *8*, 2101739; e) D. Li, W. Nie, L. Chen, D. McCoul, D. Liu, X. Zhang, Y. Ji, B. Yu, C. He, *J. Biomed. Nanotechnol.* **2018**, *14*, 2003; f) J. Liao, K. Shi, Y. Jia, Y. Wu, Z. Qian, *Bioact. Mater.* **2021**, *6*, 2221; g) J. Long, W. Zhang, Y. Chen, B. Teng, B. Liu, H. Li, Z. Yao, D. Wang, L. Li, X. F. Yu, L. Qin, Y. Lai, *Biomaterials* **2021**, *275*, 120950; h) J. W. Lu, F. Yang, Q. F. Ke, X. T. Xie, Y. P. Guo, *Nanomedicine* **2018**, *14*, 811; i) Y. Lu, L. Li, M. Li, Z. Lin, L. Wang, Y. Zhang, Q. Yin, H. Xia, G. Han, *Bioconjugate Chem.* **2018**, *29*, 2982; j) W. E. G. Müller, M. Ackermann, B. Al-Nawas, L. A. R. Righesso, R. Muñoz-Espí, E. Tolba, M. Neufurth, H. C. Schröder, X. Wang, *Acta Biomater.* **2020**, *118*, 233; k) L. Wang, Q. Yang, M. Huo, D. Lu, Y. Gao, Y. Chen, H. Xu, *Adv. Mater.* **2021**, *33*, 2100150; l) C. Yang, H. Ma, Z. Wang, M. R. Younis, C. Liu, C. Wu, Y. Luo, P. Huang, *Adv. Sci.* **2021**, *8*, 2100894; m) Q. Yang, H. Yin, T. Xu, D. Zhu, J. Yin, Y. Chen, X. Yu, J. Gao, C. Zhang, Y. Chen, Y. Gao, *Small* **2020**, *16*, 1906814; n) M. Yao, Q. Zou, W. Zou, Z. Xie, Z. Li, X. Zhao, C. Du, *Biomater. Sci.* **2021**, *9*, 3319; o) J. Yin, S. Pan, X. Guo, Y. Gao, D. Zhu, Q. Yang, J. Gao, C. Zhang, Y. Chen, *Nano-Micro Lett.* **2021**, *13*, 30; p) D. Zhang, S. Cheng, J. Tan, J. Xie, Y. Zhang, S. Chen, H. Du, S. Qian, Y. Qiao, F. Peng, X. Liu, *Bioact. Mater.* **2022**, *17*, 394; q) Z. F. Zhou, T. W. Sun, F. Chen, D. Q. Zuo, H. S. Wang, Y. Q. Hua, Z. D. Cai, J. Tan, *Biomaterials* **2017**, *121*, 1; r) C. Zhu, M. He, D. Sun, Y. Huang, L. Huang, M. Du, J. Wang, J. Wang, Z. Li, B. Hu, Y. Song, Y. Li, G. Feng, L. Liu, L. Zhang, *ACS Appl. Mater. Interfaces* **2021**, *13*, 47327; s) H. Zhuang, C. Qin, M. Zhang, J. Ma, D. Zhai, B. Ma, N. Ma, Z. Huan, C. Wu, *Biofabrication* **2021**, *13*, 045010; t) F. Yang, J. Lu, Q. Ke, X. Peng, Y. Guo, X. Xie, *Sci. Rep.* **2018**, *8*, 7345.

[47] K. S. Nørregaard, H. J. Jürgensen, H. Gårdsvoll, L. H. Engelholm, N. Behrendt, K. Søe, *Int. J. Mol. Sci.* **2021**, *22*, 6865.

[48] B. Tan, Y. Wu, Y. Wu, K. Shi, R. Han, Y. Li, Z. Qian, J. Liao, *ACS Appl. Mater. Interfaces* **2021**, *13*, 31542.

[49] R. D. Roberts, M. M. Lizardo, D. R. Reed, P. Hingorani, J. Glover, W. Allen-Rhoades, T. Fan, C. Khanna, E. A. Sweet-Cordero, T. Cash, M. W. Bishop, M. Hegde, A. R. Sertil, C. Koelsche, L. Mirabello, D. Malkin, P. H. Sorensen, P. S. Meltzer, K. A. Janeway, R. Gorlick, B. D. Crompton, *Cancer* **2019**, *125*, 3514.

[50] C. Bailly, X. Thuru, B. Quesnel, *NAR Cancer* **2020**, *2*, zcaa002.

[51] a) P. Dosta, A. M. Cryer, M. Prado, M. Z. Dion, S. Ferber, S. Kalash, N. Artzi, *Adv. Nanobiomed. Res.* **2021**, *1*, 2100006; b) P. Dosta, A. M. Cryer, M. Z. Dion, T. Shiraishi, S. P. Langston, D. Lok, J. Wang, S. Harrison, S. Ferber, S. Kalash, M. Prado, A. L. Rodríguez, A. O. Abu-Yousif, N. Artzi, *Research Square* **2022**, https://doi.org/10.21203/rs.3.rs-1647238/v1.

[52] J. A. Morcuende, P. Gomez, J. Stack, G. Oji, J. Martin, D. C. Fredericks, J. A. Buckwalter, *Iowa Orthop. J.* **2004**, *24*, 36.

[53] G. R. Mundy, *Nat. Rev. Cancer* **2002**, *2*, 584.

[54] a) F. E. Freeman, M. Haugh, L. McNamara, *J. Tissue Eng. Regener. Med.* **2013**, ; b) F. E. Freeman, M. G. Haugh, L. McNamara, *Tissue Eng., Part A* **2015**, *21*, 1320; c) F. E. Freeman, H. Stevens, P. Owens, R. Guldberg, L. McNamara, *Tissue Eng., Part A* **2016**, *22*, 1176 .

[55] F. E. Freeman, D. J. Kelly, *Sci. Rep.* **2017**, *7*, 17042.

[56] E. B. Dolan, M. G. Haugh, D. Tallon, C. Casey, L. M. McNamara, *J. R. Soc., Interface* **2012**, *9*, 3503.

[57] F. E. Freeman, D. C. Browe, J. Nulty, S. Von Euw, W. L. Grayson, D. J. Kelly, *Eur. Cells Mater.* **2019**, *38*, 168.

[58] J. Nulty, R. Burdis, D. J. Kelly, *Front. Bioeng. Biotechnol.* **2021**, *9*, 661989.

[59] Y. Zhang, P. Dosta, J. Conde, N. Oliva, M. Wang, N. Artzi, *Adv. Healthcare Mater.* **2020**, *9*, 1901101.

[60] Y. Wu, M. Crawford, Y. Mao, R. J. Lee, I. C. Davis, T. S. Elton, L. J. Lee, S. P. Nana-Sinkam, *Mol. Ther. Nucleic Acids* **2013**, *2*, 84.